
Flatten Graphs as Sequences: Transformers are Scalable Graph Generators

Dexiong Chen¹ Markus Krimmel¹ Karsten Borgwardt¹

Abstract

We introduce AUTOGRAPH, a novel autoregressive framework for generating large attributed graphs using decoder-only transformers. At the core of our approach is a reversible “flattening” process that transforms graphs into random sequences. By sampling and learning from these sequences, AUTOGRAPH enables transformers to model and generate complex graph structures in a manner akin to natural language. In contrast to diffusion models that rely on computationally intensive node features, our approach operates exclusively on these sequences. The sampling complexity and sequence length scale linearly with the number of edges, making AUTOGRAPH highly scalable for generating large sparse graphs. Empirically, AUTOGRAPH achieves state-of-the-art performance across diverse synthetic and molecular graph generation benchmarks, while delivering a 100-fold generation and a 3-fold training speedup compared to leading diffusion models. Additionally, it demonstrates promising transfer capabilities and supports substructure-conditioned generation without additional fine-tuning. By extending language modeling techniques to graph generation, this work paves the way for developing graph foundation models.

1. Introduction

Recent advancements in deep generative models have revolutionized various domains of artificial intelligence, demonstrating remarkable capabilities in generating complex data types such as images (Rombach et al., 2022), natural language (Brown et al., 2020; Touvron et al., 2023a;b), and audio (Dhariwal et al., 2020; Huang et al., 2024). These achievements have been primarily driven by the development of advanced architectures or methods such as transformers and diffusion models, alongside increasingly large-scale data resources. However, the generation of graph-

structured data, which is fundamental to numerous scientific applications including drug discovery (Vignac et al., 2023; Lim et al., 2020), protein design (Ingraham et al., 2019), and program synthesis (Brockschmidt et al., 2019), remains a significant challenge. This disparity primarily stems from the inherent complexity of preserving structural validity, maintaining invariance properties within graphs, and achieving scalability in real-world graph generation tasks.

To this end, diffusion-based models have emerged as a promising direction for graph generation, demonstrating effectiveness in synthesizing both classic unattributed graphs and molecules (Jo et al., 2022; Vignac et al., 2023). These approaches typically implement a denoising process in discrete graph space, simultaneously predicting edge connectivity and attributes. Yet, their practical applications are constrained by fundamental scalability limitations. The requirement for full adjacency matrix operations imposes quadratic memory complexity with respect to the number of nodes. Moreover, computing additional features in each denoising step such as spectral features, often involving cubic complexity, further increases the computational overhead.

Autoregressive approaches represent an alternative paradigm, constructing graphs sequentially by generating nodes and edges in a step-by-step manner (Liao et al., 2019; You et al., 2018). These models have demonstrated strong performance in generating small to medium-sized graphs by leveraging their ability to maintain structural validity through the generation process. Nevertheless, these models face inherent limitations: they require specialized architectures, primarily based on recurrent neural networks, to process the complex ad-hoc sequential representations of graphs, preventing them from directly leveraging the remarkable advances in large language models (LLMs). Moreover, these specialized architectures often struggle with long-range dependencies and ensuring global structural consistency, leading to significantly inferior performance compared to recent diffusion models (Vignac et al., 2023). This architectural constraint not only limits their scalability but also creates a growing performance gap as general-purpose LLMs continue to advance rapidly.

In light of these challenges, we introduce a novel paradigm that bridges the gap between graph generation and LLMs through a graph-to-sequence transformation. Our approach

¹Max Planck Institute of Biochemistry, Martinsried, Germany. Correspondence to: Dexiong Chen <dchen@biochem.mpg.de>.

fundamentally reconceptualizes graphs as sequential structures while maintaining their topological properties. Instead of requiring specialized architectures or operating on graph structures, we propose a method to linearize graphs into random sequences that encode local connectivity patterns. This transformation enables direct utilization of language models for graph generation while achieving optimally linear complexity with respect to the number of edges in both computational and memory requirements. Our approach effectively addresses the limitations of both diffusion-based and autoregressive methods: it maintains structural validity while enabling efficient scaling to large graphs and leveraging the powerful capabilities of modern language models.

Our work presents several technical contributions to the field of graph generation. (1) We introduce the concept of segmented Eulerian neighborhood trails (SENTs), a specialized class of Eulerian trails that permit breaks and incorporate neighborhood information. We establish sufficient conditions under which they can be employed for effective graph generation. (2) We propose an efficient flattening algorithm that transforms graphs into sequences and vice versa by sampling these SENTs, enabling lossless sequence representation of graphs. (3) Our method, termed AUTOGRAPH, achieves state-of-the-art (SOTA) performance across diverse synthetic and molecular graph generation benchmarks, delivering a 100-fold generation and a 3-fold training speedup compared to diffusion-based models while maintaining the ability to scale to graphs of possibly immense size. (4) Additionally, AUTOGRAPH demonstrates strong transfer learning capabilities and supports substructure-conditioned generation without additional fine-tuning. Our work not only advances the field of graph generation but also opens new avenues for applying LLMs to graph-centric tasks, paving the way for building foundation models for graphs.

2. Methods

In this section, we present an approach to transforming graphs into sequences, enabling their modeling akin to natural language. Our method hinges on a specialized class of random trail segments that ensure complete graph coverage. We begin by introducing the concept of segmented Eulerian trails (SET) and demonstrate theoretically why this representation alone is insufficient for effective graph generation. Subsequently, we propose an extension of SET, namely the segmented Eulerian neighborhood trail (SENT), which additionally incorporates neighborhood information alongside the trails. We elucidate sufficient conditions for effective generation and develop an efficient sampling strategy to obtain such SENTs. The section concludes with extensions and discusses how to model the SENTs autoregressively using language models, thus bridging the gap between graph learning and language modeling paradigms. An overview

of AUTOGRAPH is illustrated in Figure 1, and backgrounds and proofs are provided in Appendix C and D.

2.1. Segmented Eulerian Trail

To formalize our approach, we begin by introducing fundamental concepts in graph theory. Let V be a set of vertices and $E := V \times V$ a set of edges. A graph is defined as a tuple $G = (V_G, E_G)$, where $V_G \subseteq V$ is a finite set of vertices and $E_G \subseteq V_G \times V_G$ is the set of edges. For simplicity and without loss of generality, we restrict our attention to undirected graphs without isolated vertices, where each edge is represented as an unordered pair (u, v) for $u, v \in V$. We begin by defining the concept of a trail in a graph:

Definition 2.1 (Walk and trail). A walk is a sequence of nodes connected by edges in G and a trail is a walk in which all edges are distinct. Given a graph G , the set of trails in G is denoted as \mathcal{T}_G .

Next, we generalize the concept of trails beyond the context of a specific graph:

Definition 2.2 (Generalized trail). A generalized trail of length k is defined as a sequence of nodes $w := (w_0, \dots, w_k) \in V^{k+1}$ for $k \geq 0$ s.t. $(w_{i-1}, w_i) \neq (w_{j-1}, w_j), \forall i, j \in [k]$ and $i \neq j$.

The set of all generalized trails is denoted as \mathcal{T} , noting that $\mathcal{T}_G \subseteq \mathcal{T}$ for any G . For a generalized trail $w \in \mathcal{T}$, we define $V_w \subseteq V$ and $E_w \subseteq E$ as the sets of vertices and edges traversed by w , respectively, termed the *generated sets* of w . An *Eulerian trail* is a trail that visits every edge in a graph exactly once. Such trails are of particular interest as they capture the complete topology of the graph. However, the existence of an Eulerian trail depends on specific conditions related to vertex degrees and connectivity (Biggs et al., 1986). To generalize this concept to arbitrary graphs, we introduce the notion of trail segments:

Definition 2.3 (Segmented Eulerian trail (SET)). A segmented Eulerian trail (SET) in G is a sequence of trail segments such that each edge is visited exactly once across all segments, and segments do not need to be connected. Formally, a SET of size k in G is defined as $s := (s_1, \dots, s_k)$ s.t. $s_i \in \mathcal{T}_G$, and the generated edge sets of its segments form a partition of E_G , i.e., $\cup_{i=1}^k E_{s_i} = E_G$ and $E_{s_i} \cap E_{s_j} = \emptyset, \forall i, j \in [k], i \neq j$. Similarly, a SET (without relying on a specific graph) is defined as a sequence of generalized trails whose generated edge sets are disjoint.

The set of all SETs in G is denoted as \mathcal{S}_G , and the set of all SETs is denoted as \mathcal{S} . For a SET $s = (s_i)_{i=1}^k$, we define the *generated node and edge sets* as $V_s := \cup_{i=1}^k V_{s_i}$ and $E_s := \cup_{i=1}^k E_{s_i}$. The graph $G_s := (V_s, E_s)$ is termed *generated graph* of s . It is easy to show that s is a SET in G if $G_s \simeq G$. Moreover, SETs can be classified into equivalence classes based on graph isomorphism, as formalized below:

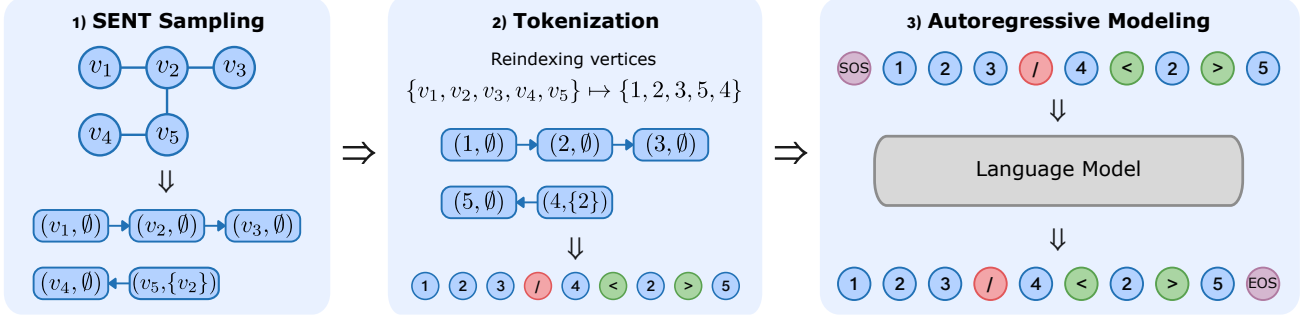


Figure 1. Overview of AUTOGRAPH: (1) We use Algorithm 1 to sample a SENT s from the input graph: $s = (s_1, s_2)$ with $s_1 = ((v_1, \emptyset), (v_2, \emptyset), (v_3, \emptyset))$ and $s_2 = ((v_5, \{v_2\}), (v_4, \emptyset))$. (2) We tokenize it by reindexing the vertices based on their first occurrence order in s and adding special tokens (‘/’ represents breakage between segments, ‘<’ and ‘>’ indicate the start and end of a neighborhood set). (3) We perform the next token prediction on the tokenized sequences using a decoder-only transformer or any language model.

Definition 2.4 (SET isomorphism). For any two SETs $s, t \in \mathcal{S}$, we say they are isomorphic $s \simeq t$ if there is a bijection $\pi : V_s \rightarrow V_t$ between their generated node sets and $\pi(s) = t$ where π applies elementwise to all nodes in s .

This isomorphism partitions \mathcal{S} into equivalence classes. Moreover, we have the following relationship between SETs and graphs, relevant for our tokenization (Sec. 2.4):

Theorem 2.5. For any SETs $s, t \in \mathcal{S}$, their generated graphs are isomorphic, i.e., $G_s \simeq G_t$, if $s \simeq t$. Conversely, if two graphs $G \simeq H$, then for any SET $s \in \mathcal{S}_G$, there exists a SET $t \in \mathcal{S}_H$ s.t. $s \simeq t$.

While a SET in G fully characterizes its structure, we show below the prefixes of the SET do not necessarily describe the substructures of G , a critical property for effective autoregressive graph generation.

Definition 2.6 (Flattening). The flattening of a sequence of sequences s is the concatenation of all its sequences, denoted as $\|s$.

Definition 2.7 (Prefix of a SET). For $s \in \mathcal{S}$, we call t a prefix of s if $\|t$ is a prefix of $\|s$.

Lemma 2.8. For any graph G and SET s in G , the generated graph of any prefix of s is a subgraph of G , but not necessarily an induced subgraph.

This result motivates us to extend the definition of generalized trails to incorporate the full structural information of the induced subgraphs, rather than arbitrary subgraphs, to constrain the generation space better and address long-range dependency challenges. Without this extension, dependencies between neighboring nodes may span a long sequence of generation steps, making it more difficult for the model to learn such dependencies. Empirically, we show that SET fails to accurately generate graphs in Section 4.4.

2.2. Segmented Eulerian Neighborhood Trail

To make the prefixes of a SET encode richer information, we need to extend SET to contain neighborhood information in a graph. Thus, we consider the following definition:

Definition 2.9 (Neighborhood sequence). A neighborhood sequence is a sequence of tuples $w := (w_0, \dots, w_k)$ where $w_i = (v_i, A_i)$ with a node $v_i \in V$ and a neighborhood set $A_i \subseteq V, \forall i \in \{0, \dots, k\}$. w is called Hamiltonian if its node sequence $n(w) := (v_0, \dots, v_k)$ has non-repeated elements. Moreover, w is called causal if A_i only contains visited nodes, i.e., $A_i \subseteq \{v_0, \dots, v_{i-1}\} \forall i \in [k]$.

We now extend this to trails:

Definition 2.10 (Neighborhood trail). A neighborhood trail is a neighborhood sequence that satisfies two conditions. (i) $n(w)$ is a generalized trail. (ii) If we define the generated edge set of w_i as $E_{w_i} = \{(v_i, u) \mid u \in A_i\}$, the family $\{E_{n(w)}, E_{w_1}, \dots, E_{w_k}\}$ is pairwise disjoint. Its union is called the generated edge set of w .

The set of all neighborhood trails is denoted by $\mathcal{T}^{\mathcal{N}}$. For any $w \in \mathcal{T}^{\mathcal{N}}$, we denote by $G_w := (V_w, E_w)$ the generated graph of w where $V_w := (\cup_{i=1}^k A_i) \cup V_{n(w)}$ is the generated node set and E_w is the generated edge set. Note that a generalized trail is a neighborhood trail with $A_i = \emptyset, \forall i$. We extend SET to incorporate neighborhood information:

Definition 2.11 (Segmented Eulerian neighborhood trail (SENT)). A segmented Eulerian neighborhood trail (SENT) of size k is a sequence of neighborhood trails $s := (s_1, \dots, s_k)$ with pairwise disjoint generated edge sets, i.e., $s_i \in \mathcal{T}^{\mathcal{N}}$ and $E_{s_i} \cap E_{s_j} = \emptyset, \forall i, j \in [k], i \neq j$.

Similarly to SETs, the generated graph of a SENT s is denoted by $G_s = (V_s, E_s)$. If a graph $G \simeq G_s$, we say that s is a SENT in G . We denote by $\mathcal{S}^{\mathcal{N}}$ and $\mathcal{S}_G^{\mathcal{N}}$ the set of SENTs and SENTs in G . Analogously to SETs, we define an isomorphism over $\mathcal{S}^{\mathcal{N}}$ and obtain the same relationship as in Thm. 2.5. A prefix of a SENT is defined similarly to

that of a SET. We give below conditions to force generated graphs of prefixes of a SENT to be induced subgraphs.

Definition 2.12 (Causal SENT). A SENT s is called causal if its flattening $\|s$ is causal.

Definition 2.13 (Hamiltonian and semi-hamiltonian SENT). A SENT s is called Hamiltonian if its flattening $\|s$ is Hamiltonian. s is called semi-hamiltonian if s is Hamiltonian, or for any nodes visited more than once, their occurrences after the first time should be in a start tuple of a neighborhood trail and their associated neighborhood sets are empty.

Theorem 2.14. For any causal SENT $s \in \mathcal{S}^{\mathcal{N}}$, the generated graph of any prefix t of s is an induced subgraph of G_s if and only if s is semi-hamiltonian. In this case, s is called subgraph-induced.

Now let us find the conditions for a causal and Hamiltonian SENT. For any SENT s and a tuple $w := (v, A)$ in s , we denote by $V_s(w)$ the set of nodes visited by s before w , excluding the node linked to v through the trail if it exists. We have the following necessary and sufficient conditions:

Theorem 2.15. For $s \in \mathcal{S}_G^{\mathcal{N}}$, s is causal and Hamiltonian if and only if every tuple $w := (v, A_v)$ in $\|s$ satisfies $A_v = \mathcal{N}_G(v) \cap V_s(w)$. In this case, every node is visited exactly once. Moreover, s is causal and semi-hamiltonian if and only if every tuple $w := (v, A_v)$ in s satisfies either $A_v = \mathcal{N}_G(v) \cap V_s(w)$ or $A_v = \emptyset$.

This theorem offers a simple sufficient condition for subgraph-induced SENTs. We provide in the following an implementation through a random path sampling strategy.

2.3. Sampling Algorithm for SENT

Thm. 2.15 offers a simple strategy to sample a causal and Hamiltonian SENT: one needs to traverse the graph and choose the neighborhood set as all neighbors of the current node that have been visited. The traversing strategy could be achieved through a random path sampling or a depth-first search. In Algorithm 1, we provide a sampling strategy based on random path sampling with breaks.

Complexity analysis. The length of a SENT including the sizes of neighborhood sets (in other words, tokenized SENT defined in Section 2.4) is bounded by the number of edges as it can visit each edge only once. Therefore, both the time and space complexity of sampling a SENT from graph G are $\mathcal{O}(m)$ where m is the number of edges.

2.4. Tokenization of SENT

Previous works have explored related concepts of sequences in graphs. For example, You et al. (2018) investigated causal Hamiltonian neighborhood sequences generated through breadth-first search, while Liao et al. (2019); Goyal et al. (2020) constructed SENT-like sequences using depth-first

Algorithm 1 Causal and Hamiltonian SENT Sampling

Input: $G = (V, E)$

Output: A SENT s in G

```

1: Set of unvisited nodes  $U \leftarrow V$ 
2:  $s \leftarrow []$ 
3:  $v \leftarrow \text{RandomSample}(U); U \leftarrow U \setminus \{v\}$ 
4:  $t \leftarrow [(v, \emptyset)]$  ▷ first neighborhood trail
5: while  $U \neq \emptyset$  do
6:   if  $\mathcal{N}_G(v) \cap U = \emptyset$  then ▷ start a new trail
7:      $s.append(t)$ 
8:      $v \leftarrow \text{RandomSample}(U); U \leftarrow U \setminus \{v\}$ 
9:      $A \leftarrow \mathcal{N}_G(v) \cap (V \setminus U)$ 
10:     $t \leftarrow [(v, A)]$ 
11:   else ▷ sample the next node in the trail
12:      $u \leftarrow \text{RandomSample}(\mathcal{N}_G(v) \cap U)$ 
13:      $U \leftarrow U \setminus \{u\}$ 
14:      $A \leftarrow (\mathcal{N}_G(u) \setminus \{v\}) \cap (V \setminus U)$ 
15:      $t.append((u, A))$ 
16:      $v \leftarrow u$ 

```

search. However, neither of these works interpreted these sequences as a language. Here, we present a method to bridge the gap between graph generation and language modeling.

The tokenization process starts by mapping all isomorphic SENTs to the same sequence, by reindexing the vertices according to their first occurrence order within the sequence. Specifically, if we denote this ordering function for a SENT s by $\pi : V_s \rightarrow \{1, \dots, |V_s|\}$, s is then replaced with its ordered representation $\pi(s)$. Thanks to the isomorphism property of SENT (Thm. 2.5), $\pi(s)$ generates a graph isomorphic to G_s while ensuring the obtained sequence invariant to the node ordering of the input graph.

To convert an (ordered) SENT into a machine-readable sequence, we tokenize it into a sequence of indices using special tokens. These tokens include symbols such as ‘/’ to indicate a breakage between segments, and ‘<’ and ‘>’ to mark the start and end of a neighborhood set. Specifically, for any $s := (s_1, \dots, s_k) \in \mathcal{S}^{\mathcal{N}}$, we define the tokenization function `Token` as follows:

$$\text{Token}(s) := \text{Token}(s_1) \parallel [/] \parallel \dots \parallel [/] \parallel \text{Token}(s_k),$$

where

$$\text{Token}(s_i) := \parallel_{w \in s_i} \text{Token}(w),$$

and for each tuple $w := (v, A)$ with the sorted set $A = \{u_1, \dots, u_p\}$ (due to the reindexing by π), we define:

$$\text{Token}(w) := [v, <, u_1, \dots, u_p, >].$$

This process converts a SENT into a sequence of tokens that a language model can effectively model. Using an equivalent form, the resulting tokenization induces a *non-Markovian* random walk in the graph, incorporating additional virtual nodes labeled with the above special tokens

(see Appendix C.2 for more details). *Language modeling of SENTs aims to learn the state transition probabilities.*

2.5. Extension to Attributed Graphs

Our method can be easily extended to graphs with categorical (or discretized) attributes by inserting node and edge attributes in an interleaved fashion into the tokenized SENT sequence. Specifically, let $L_{\text{node}}(v)$ and $L_{\text{edge}}(u, v)$ be the attributes of a node v and an edge (u, v) respectively. Using the same notation as above, we define for any $s_i := (w_1, \dots, w_q) \in \mathcal{T}^{\mathcal{N}}$ with $w_i = (v_i, \cdot)$:

$$\text{Token}(s_i) := \text{Token}(w_1) \parallel [L_{\text{edge}}(v_1, v_2)] \parallel \text{Token}(w_2) \parallel \dots \parallel \text{Token}(w_q),$$

$$\text{Token}(w) := [v, L_{\text{node}}(v), <, L_{\text{edge}}(v, u_1), u_1, \dots, L_{\text{edge}}(v, u_p), u_p, >].$$

2.6. Autoregressive Modeling of Tokenized SENTs

The sampling and tokenization of SENTs in graphs allows for transforming graphs into sequences, which could be modeled by language models. Specifically, given a graph G represented as a SENT s , which consists of a sequence of tokens (s_1, \dots, s_n) , a standard language modeling objective is to maximize the following log-likelihood:

$$p(s) = \sum_{i=1}^n \log p_{\theta}(s_i | s_1, \dots, s_{i-1}), \quad (1)$$

where the conditional probability p_{θ} is modeled using a neural network with parameters θ . The architecture of the neural network can be any SOTA sequence model.

3. Related Work

Autoregressive models for graph generation. Autoregressive models generate graphs by sequentially adding nodes and edges. GraphRNN (You et al., 2018) pioneered this approach by framing graph generation as a sequence prediction task, demonstrating the capacity of recurrent neural networks (RNNs) (Chung et al., 2014) to capture complex structures. DeepGMG (Li et al., 2018) introduced a probabilistic policy framework for conditional generation, while GRAN (Liao et al., 2019) and BiGG (Dai et al., 2020) enhanced efficiency and scalability by generating multiple nodes and edges in parallel.

Recent research has focused on optimizing the generation order. Chen et al. (2021) highlighted that the ordering of node and edge additions impacts graph quality, and GraphARM (Kong et al., 2023) applied reinforcement learning to dynamically refine this order. Goyal et al. (2020) incorporated logical constraints to improve domain-specific generation, and Bacciu et al. (2020) proposed Bayesian reasoning to better capture graph dependencies.

Although these models have shown to be efficient and effective in synthetic datasets, they face inherent unification limitations, reducing their applicability to large-scale real-world datasets. Our proposed unified and powerful sequence representation of graphs aims to address these challenges.

Other graph generative models. Other graph generative models include variational, GAN-based, and diffusion-based approaches. GraphVAEs (Kipf & Welling, 2016; Simonovsky & Komodakis, 2018) employ variational autoencoders to learn continuous latent representations, effectively generating small graphs but struggling with more complex structures. GAN-based models, such as NetGAN (Bojchevski et al., 2018) and SPECTRE (Martinkus et al., 2022), generate graphs by modeling graph descriptors like random walks and spectral features.

Diffusion-based models iteratively refine noise into structured graphs through reverse diffusion steps. Continuous diffusion models (Niu et al., 2020; Jo et al., 2022) adapt denoising diffusion probabilistic models for graph generation. To leverage graph sparsity and structure, discrete diffusion models (Vignac et al., 2023; Kong et al., 2023) have been developed. However, a key challenge for these models is the slow sampling process due to the long reverse diffusion chain. To mitigate this limitation, several efficient diffusion techniques have been proposed, including EDGE (Chen et al., 2023), HiGen (Karami, 2024), ESGG (Bergmeister et al., 2024), and Pard (Zhao et al., 2024).

Random walks for graph learning. Random walks have been widely used in graph learning due to their strong expressive power. GCKN (Chen et al., 2020) and RWGNN (Nikolentzos & Vazirgiannis, 2020) utilize path and walk kernels to learn graph representations. Several recent works (Ivanov & Burnaev, 2018; Wang et al., 2021; Yin et al., 2022) explicitly integrate random walk sequences with positional encodings, inspiring subsequent methods such as CRaWL (Tönshoff et al., 2023), NeuralWalker (Chen et al., 2024) and RWNN (Kim et al., 2024), which further enhance graph representation learning via random walk sequence modeling. GraphGPT (Zhao et al., 2023) leverages Eulerian paths to improve graph property prediction. Our work uniquely explores random sequence representations of graphs focusing on graph generation, introducing a novel perspective on combining random walks and language modeling for scalable graph generative modeling.

4. Experiments

In this section, we evaluate the performance of AUTOGRAPH on several graph generation benchmarks, including both small and large graphs, and synthetic and real-world molecular datasets. Our experiments compare its performance to several SOTA methods and particularly focus on evaluating the following aspects: (1) We show its ability to

Table 1. Comparison of AUTOGRAPH to SOTA methods on Planar

MODEL	PLANAR GRAPHS $n_{\text{graphs}} = 128, V = 64$					
	DEG.	CLUS.	ORBIT	SPEC.	RATIO	VUN
TRAINING SET	0.0002	0.0310	0.0005	0.0038	1.0	-
GRAPHRNN	0.0049	0.2779	1.2543	0.0459	638.5	0.0
GRAN	0.0007	0.0426	0.0009	0.0075	2.1	0.0
SPECTRE	0.0005	0.0785	0.0012	0.0112	2.6	25.0
EDGE	0.0761	0.3229	0.7737	0.0957	490.9	0.0
DiGRESS	0.0007	0.0780	0.0079	0.0098	6.1	77.5
ESGG	0.0005	0.0626	0.0017	0.0075	2.5	95.0
AUTOGRAPH	0.0004	0.0605	0.0003	0.0064	1.5	87.5

generate relatively small graphs with a 100-fold inference speedup compared to diffusion-based models while maintaining or even improving structural validity. (2) We show its ability to scale to large graphs without loss of performance. (3) We demonstrate its effectiveness in generating real-world graphs with attributes with a focus on molecular generation, outperforming SOTA diffusion models. (4) We showcase its strong transfer capabilities and its ability to perform substructure-conditioned generation without any additional fine-tuning. Additional details on experimental settings and evaluation are provided in Appendix E.

Implementation details. We employ the LLaMA model with 12 layers and a hidden dimension of 768 as our sequence model backbone across all experiments, aligning with the architecture of GPT-2’s smallest variant (Radford et al., 2019). Although prior works have used smaller models, we argue that our approach still demonstrates better scalability and faster training and inference speeds compared to diffusion models. For inference, we adopt the commonly used top-k sampling strategy (Fan et al., 2018). Our implementation leverages the Hugging Face framework (Jain, 2022), providing users with a flexible interface to experiment with SOTA language models for graph generation.

Evaluation. For fair comparison, we align our evaluation methodology with established practices from prior works (You et al., 2018; Martinkus et al., 2022; Vignac et al., 2023). Our evaluation compares generated samples against the test set using maximum mean discrepancy (MMD) (Gretton et al., 2012), computed across multiple graph descriptors: node degree distributions (DEG.), clustering coefficients (CLUS.), orbit count statistics (ORBIT), and eigenvalue spectra (SPEC.). As a reference, we also compute these metrics on the training set and report the mean ratio across all properties (RATIO).

For synthetic datasets, we additionally assess model performance using the VUN metric, the proportion of generated graphs that are valid, unique, and novel. Our efficiency analysis includes two measurements: inference speed, calculated as the per-graph generation time when producing 1024 graphs, and training efficiency, measured as the time required to achieve a VUN score of 75.0 for the Planar dataset and 60.0 for the SBM dataset. All efficiency measurements are performed on one NVIDIA H100 GPU.

Table 2. Comparison of AUTOGRAPH to SOTA methods on SBM

MODEL	STOCHASTIC BLOCK MODELS $n_{\text{graphs}} = 128, V _{\text{max}} = 187, V _{\text{avg}} \approx 104$					
	DEG.	CLUS.	ORBIT	SPEC.	RATIO	VUN
TRAINING SET	0.0008	0.0332	0.0255	0.0027	1.0	-
GRAPHRNN	0.0055	0.0584	0.0785	0.0065	3.5	5.0
GRAN	0.0113	0.0553	0.0540	0.0054	5.0	25.0
SPECTRE	0.0015	0.0521	0.0412	0.0056	1.8	52.5
EDGE	0.0279	0.1113	0.0854	0.0251	12.7	0.0
DiGRESS	0.0018	0.0485	0.0415	0.0045	1.8	60.0
ESGG	0.0119	0.0517	0.0669	0.0067	5.4	45.0
AUTOGRAPH	0.0077	0.0519	0.0439	0.0040	3.4	92.5

Table 3. Time comparison of AUTOGRAPH to representative models. OOT indicates the model never reaches the target VUN.

DATASET	TIME	DiGRESS	GRAN	ESGG	AUTOGRAPH
PLANAR	TRAINING	25.9h	OOT	7.4h	6.2h (4.2×)
	INFERENCE	2.84s	0.03s	4.60s	0.01s (284×)
SBM	TRAINING	47.7h	OOT	OOT	13.8h (3.5×)
	INFERENCE	13.05s	0.13s	30.0s	0.14s (93×)

For molecular generation datasets, we strictly follow the evaluation metrics used in DiGress (Vignac et al., 2023). More details about evaluation are provided in Appendix E.2.

4.1. Comparison to State-of-the-Art Methods

We evaluate the performance of AUTOGRAPH compared to other SOTA graph generative models using the standard setting without pre-training.

4.1.1. SMALL SYNTHETIC GRAPH GENERATION

We first evaluate our method on the small synthetic graph datasets introduced by Martinkus et al. (2022), including the Planar and SBM datasets. We compare the performance of AUTOGRAPH against GraphRNN (You et al., 2018), GRAN (Liao et al., 2019), SPECTRE (Martinkus et al., 2022), EDGE (Chen et al., 2023), DiGress (Vignac et al., 2023), ESGG (Bergmeister et al., 2024). As shown in Tables 1 and 2, AUTOGRAPH achieves the best and second-best MMD ratios on average while ranking second-best and best in terms of VUN scores for the Planar and SBM datasets, respectively. Notably, all previous methods exhibit limited structural validity on the SBM dataset, with the best VUN scores reaching only 60.0.

Additionally, we assess the training and inference times of AUTOGRAPH against representative models, including DiGress, GRAN, and ESGG. As presented in Table 3, AUTOGRAPH is approximately 3 times faster during training and 100 times faster during inference compared to diffusion-based models. This substantial speedup over diffusion-based models is even more pronounced than that observed in other data modalities such as images (Tian et al., 2024).

4.1.2. LARGE GRAPH GENERATION

To understand the scalability of AUTOGRAPH, we evaluate its performance on the Proteins and Point Clouds datasets

Table 4. Comparison of AUTOGRAPH to SOTA methods on the Proteins and Point Clouds datasets. OOM indices out of memory.

MODEL	PROTEINS $n_{\text{graphs}} = 587, V _{\text{max}} = 500, V _{\text{avg}} \approx 258$					POINT CLOUDS $n_{\text{graphs}} = 26, V _{\text{max}} = 5037, V _{\text{avg}} \approx 1332$				
	DEG.	CLUS.	ORBIT	SPEC.	RATIO	DEG.	CLUS.	ORBIT	SPEC.	RATIO
TRAINING SET	0.0003	0.0068	0.0032	0.0005	1.0	0.0000	0.1768	0.0049	0.0043	1.0
GRAPHRNN	0.0040	0.1475	0.5851	0.0152	62.1	OOM	OOM	OOM	OOM	OOM
GRAN	0.0479	0.1234	0.3458	0.0125	77.7	0.0201	0.4330	0.2625	0.0051	19.1
SPECTRE	0.0056	0.0843	0.0267	0.0052	12.5	OOM	OOM	OOM	OOM	OOM
EDGE	0.1863	0.3406	0.6786	0.1075	274.5	0.4441	0.3298	1.0730	0.4006	104.7
DiGRESS	0.0041	0.0489	0.1286	0.0018	16.2	OOM	OOM	OOM	OOM	OOM
ESGG	0.0030	0.0309	0.0047	0.0013	4.7	0.0139	0.5775	0.0780	0.0055	6.8
AUTOGRAPH	0.0004	0.0244	0.0056	0.0013	2.3	0.0307	0.3031	0.0167	0.0171	3.0

Table 5. Comparison of AUTOGRAPH to SOTA methods on QM9

MODEL	QM9 WITH HYDROGEN ATOMS $n_{\text{graphs}} = 100\text{K}, V _{\text{max}} = 29, V _{\text{avg}} \approx 18$				
	VALID \uparrow	UNIQUE \uparrow	NOVEL \uparrow	ATOM STABLE \uparrow	MOL STABLE \uparrow
DiGRESS	95.4	97.6	33.4	98.1	79.8
AUTOGRAPH	97.7	96.7	45.5	98.6	87.3

used by Liao et al. (2019). The results, shown in Table 4, demonstrate that even when using a context window shorter than the longest sequence sampled from the dataset, AUTOGRAPH achieves MMD ratios comparable to those observed on the Planar and SBM datasets. Furthermore, AUTOGRAPH outperforms all existing methods in terms of MMD ratio, achieving a twofold or more improvement over the previous best model, ESGG. More significantly, while ESGG was specifically designed for generating unattributed graphs, AUTOGRAPH demonstrates versatility by being applicable to both unattributed and attributed graphs.

4.1.3. MOLECULAR GRAPH GENERATION

We demonstrate the applicability of our method to generating real-world attributed graphs, such as molecular structures. We evaluate AUTOGRAPH on the same datasets used by DiGress (Vignac et al., 2023), including QM9 (all atoms) (Wu et al., 2018), MOSES (Polykovskiy et al., 2020), and GuacaMol (Brown et al., 2019). Following the data splits and experimental setup from DiGress, we benchmark AUTOGRAPH against a variety of SOTA models, including DiGress, VAE on SMILES (Polykovskiy et al., 2020), JT-VAE (Jin et al., 2018), GraphINVENT (Mercado et al., 2021), NAGVAE (Kwon et al., 2020), LSTM and MCTS (Brown et al., 2019). On the QM9 dataset (Table 5), AUTOGRAPH outperforms DiGress across all metrics except uniqueness, showing its superiority for attributed graphs.

For the more challenging MOSES and GuacaMol datasets, AUTOGRAPH also demonstrates superior performance, achieving higher validity and improved distributional alignment as measured by metrics like FCD, as shown in Tables 6 and 7. Notably, to our best knowledge, AUTOGRAPH is the first autoregressive model for graphs to surpass diffusion-based approaches on these datasets. It is worth mentioning that all metrics were computed using SMILES repre-

Table 6. Comparison of AUTOGRAPH to SOTA methods on MOSES

MODEL	TYPE	MOSES $n_{\text{graphs}} = 1.58\text{M}, V _{\text{max}} = 27, V _{\text{avg}} \approx 22$					
		VALID \uparrow	UNIQUE \uparrow	NOVEL \uparrow	FILTERS \uparrow	SNN \downarrow	
VAE	SMILES	97.7	99.8	69.5	99.7	0.57	0.58
JT-VAE	FRAGMENTS	100	100	99.9	97.8	1.00	0.53
GRAPHINVENT	GRAPH	96.4	99.8	-	95.0	1.22	0.54
DiGRESS	GRAPH	85.7	100	95.0	97.1	1.19	0.52
AUTOGRAPH	GRAPH	87.4	100	85.9	98.6	0.91	0.55

Table 7. Comparison of AUTOGRAPH to SOTA methods on GuacaMol

MODEL	TYPE	GUACAMOL $n_{\text{graphs}} = 1.1\text{M}, V _{\text{max}} = 88, V _{\text{avg}} \approx 28$				
		VALID \uparrow	UNIQUE \uparrow	NOVEL \uparrow	KL DIV \uparrow	FCD \uparrow
LSTM	SMILES	95.9	100	91.2	99.1	91.3
NAGVAE	GRAPH	92.7	95.5	100	38.4	0.9
MCTS	GRAPH	100	100	99.4	52.2	1.5
DiGRESS	GRAPH	85.2	100	99.9	92.9	68.0
AUTOGRAPH	GRAPH	91.6	100	97.7	97.5	79.2

sentations rather than molecular graphs. Due to the non-reversible nature of converting SMILES to graphs and back, where approximately 20% of molecules cannot be mapped back to their original SMILES (Vignac et al., 2023), some discrepancies are introduced when calculating these metrics. Despite these challenges, AUTOGRAPH achieves validity and FCD scores comparable to SMILES-based methods.

Furthermore, AUTOGRAPH demonstrates remarkable efficiency, with training times of less than one day on both datasets, compared to up to one week for DiGress (Vignac et al., 2023). This substantial reduction in training time underscores AUTOGRAPH’s practical advantages in large-scale and high throughput molecular graph generation tasks.

4.2. Transfer Performance of AUTOGRAPH

We evaluate the transferability of AUTOGRAPH by pre-training it on a large dataset of synthetic graphs generated using NetworkX (Hagberg et al., 2008) and fine-tuning it on the unattributed graph datasets. Dataset and experimental details are provided in Appendix E. As shown in Table 8, the pre-trained model consistently outperforms the baseline on small synthetic datasets in terms of the VUN score, achieving near-perfect validity. On larger graph datasets, the pre-trained model also surpasses the baseline across MMD metrics, demonstrating its ability to generalize to more complex structures. However, on small synthetic datasets, the pre-trained model shows a slight decline in MMD metrics

Table 8. Transfer performance on downstream tasks using AUTOGRAPH pre-trained on the NetworkX dataset. Red and green colors indicate relative decreases and increases respectively, compared to AUTOGRAPH without pre-training.

DATASET	DEG.	CLUS.	ORBIT	SPEC.	RATIO	VUN (IMPROV.)
NETWORKX	0.0016	0.0073	0.0068	0.0020	-	-
PLANAR	0.0007	0.0811	0.0005	0.0061	2.2	95.0 (+7.5)
SBM	0.0099	0.0566	0.0854	0.0065	4.8	97.5 (+5)
PROTEINS	0.0002	0.0183	0.0038	0.0012	1.7	-
POINT CLOUDS	0.0154	0.2591	0.0076	0.0236	2.8	-

Table 9. Motif scaffolding using the motif 1,4-Dihydroquinoline.

# COPIES OF THE MOTIF	VALID	UNIQUE	NOVELTY
1	92.0	98.8	99.6
2	88.8	99.7	100.0
5	66.0	100.0	100.0

compared to the baseline. These findings highlight the potential of building foundation models for graph generation and underscore the need for more comprehensive benchmark datasets, similar to those established in other domains.

4.3. Substructure Conditioned Generation

We explore the ability of AUTOGRAPH to perform substructure-conditioned generation without requiring fine-tuning. Given a subgraph S (which could represent a functional motif of interest in drug discovery), we flatten the subgraph into a SENT sequence and condition the generation process on this sequence. This approach guarantees that the generated graph will contain S as an induced subgraph (Thm. 2.14). As a proof-of-concept, we follow the methodology of Vignac et al. (2023); Maziarz et al. (2022) and generate molecular graphs starting from a specific motif, called 1,4-Dihydroquinoline¹, using the model pre-trained on the GuacaMol dataset. Our results in Table 9 demonstrate that this approach maintains similar validity, uniqueness, and novelty to unconditional generation (Table 7). To further showcase the flexibility of this method, we test more extreme cases by replicating the same motif multiple times before performing the conditional generation. While validity decreases significantly when using an unrealistically large number of copies (e.g. 5), the model still generates some visually plausible molecules (Appendix F.3), showing superior flexibility over Vignac et al. (2023). These results highlight the potential of AUTOGRAPH for important applications in drug discovery, particularly in motif scaffolding.

4.4. Ablation Experiments

In this study, we aim to understand the effectiveness of key components in AUTOGRAPH.

Comparison of sequence model architectures. AUTOGRAPH provides a novel framework for evaluating the capability of current LLM architectures in graph generation

¹https://pubchem.ncbi.nlm.nih.gov/compound/1_4-Dihydroquinoline

Table 10. Comparison of sequence model architectures on Planar

ARCHITECTURE	DEG.	CLUS.	ORBIT	SPEC.	RATIO	VUN
GPT-2	0.0004	0.0720	0.0010	0.0053	1.8	85.0
MAMBA	0.0002	0.0429	0.0014	0.0087	1.6	55.0
LLAMA	0.0005	0.0651	0.0005	0.0056	1.6	90.0

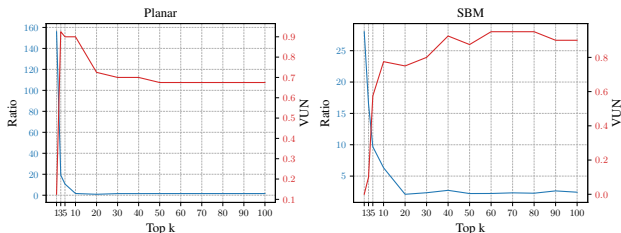


Figure 2. The effect of top-k sampling on the Planar and SBM datasets.

and, more broadly, in structural reasoning tasks. In Table 10, we compare several state-of-the-art architectures on the Planar dataset, including GPT-2 (Radford et al., 2019), Mamba (Gu & Dao, 2023), and LLaMA (Touvron et al., 2023a). While all models achieve comparable MMD ratios, transformer-based architectures, particularly LLaMA, demonstrate significantly better performance in terms of VUN scores compared to state-space models. These findings highlight the potential of AUTOGRAPH to serve as a valuable benchmark for assessing sequence/language models’ capabilities in graph generation tasks.

Effect of top-k sampling. A key advantage of AUTOGRAPH over diffusion-based approaches is the flexibility to apply top-k sampling (Fan et al., 2018) during inference, which can improve generation quality. As shown in Figure 2, a smaller k improves the VUN score on the Planar dataset, whereas it is not beneficial on the SBM dataset. In contrast, increasing k generally improves MMD ratios across both datasets. These observations suggest that top-k sampling can be optimized based on dataset characteristics. In our experiments, we select the best k that maximizes the VUN score for small synthetic datasets and minimizes the validation MMD ratios for other datasets. Importantly, this flexibility allows practitioners to select k based on the specific performance criteria they aim to prioritize.

Comparison of SET and SENT. As discussed in Section 2, SENT is preferred over SET for graph generation, as incorporating neighborhood information is essential to ensure structural coherence. To empirically validate this, we compare the performance of SENT and SET on the Planar dataset and present the training curves in Figure 3. Consistent with our theoretical analysis, SET fails to produce high-validity graphs, resulting in a VUN score close to zero, whereas SENT successfully generates valid planar graphs.

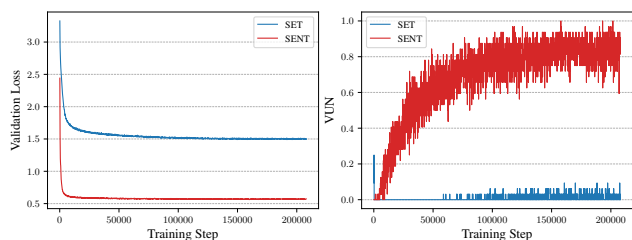


Figure 3. SET vs SENT on the Planar dataset

5. Conclusion

We proposed AUTOGRAPH, a scalable and efficient autoregressive model for attributed graph generation. AUTOGRAPH demonstrates the ability to handle large graphs while preserving high generation quality. It enables substructure-conditioned generation without requiring additional fine-tuning and shows promising transfer capabilities. More importantly, it establishes a critical connection between graph modeling and language modeling, representing a significant step toward leveraging language modeling paradigms to address challenges in graph generation or more general graph learning tasks.

Acknowledgements

The authors thank Dr. Till Hendrik Schulz, Philip Hartout, and Błażej Banaszewski for their insightful discussions and valuable feedback on the manuscript.

Impact Statement

Our research focuses on advancing the algorithmic development of graph generative models, strongly emphasizing their responsible and ethical application in specialized fields. In domains such as drug discovery and synthetic biology, ensuring the trustworthiness and appropriate use of our methods is essential to prevent potential misuse. Through our experiments, we showcase the potential of our approach in these fields, underscoring its promise to deliver meaningful societal benefits while acknowledging the need to address potential risks.

References

Bacciu, D., Micheli, A., and Podda, M. Edge-based sequential graph generation with recurrent neural networks. *Neurocomputing*, 416:177–189, 2020.

Bergmeister, A., Martinkus, K., Perraudin, N., and Wattenhofer, R. Efficient and scalable graph generation through iterative local expansion. In *International Conference on Learning Representations (ICLR)*, 2024.

Biggs, N., Lloyd, E. K., and Wilson, R. J. *Graph Theory, 1736-1936*. Oxford University Press, 1986.

Bojchevski, A., Shchur, O., Zügner, D., and Günnemann, S. Netgan: Generating graphs via random walks. In *International Conference on Machine Learning (ICML)*, pp. 610–619, 2018.

Brockschmidt, M., Allamanis, M., Gaunt, A. L., and Polozov, O. Generative code modeling with graphs. In *International Conference on Learning Representations (ICLR)*, 2019.

Brown, N., Fiscato, M., Segler, M. H., and Vaucher, A. C. Guacamol: benchmarking models for de novo molecular design. *Journal of chemical information and modeling*, 59(3):1096–1108, 2019.

Brown, T., Mann, B., Ryder, N., Subbiah, M., Kaplan, J. D., Dhariwal, P., Neelakantan, A., Shyam, P., Sastry, G., Askell, A., Agarwal, S., Herbert-Voss, A., Krueger, G., Henighan, T., Child, R., Ramesh, A., Ziegler, D., Wu, J., Winter, C., Hesse, C., Chen, M., Sigler, E., Litwin, M., Gray, S., Chess, B., Clark, J., Berner, C., McCandlish, S., Radford, A., Sutskever, I., and Amodei, D. Language models are few-shot learners. In *Advances in Neural Information Processing Systems (NeurIPS)*, volume 33, pp. 1877–1901, 2020.

Chen, D., Jacob, L., and Mairal, J. Convolutional kernel networks for graph-structured data. In *International Conference on Machine Learning (ICML)*, pp. 1576–1586, 2020.

Chen, D., Schulz, T. H., and Borgwardt, K. Learning long range dependencies on graphs via random walks. *arXiv preprint arXiv:2406.03386*, 2024.

Chen, X., Han, X., Hu, J., Ruiz, F., and Liu, L. Order matters: Probabilistic modeling of node sequence for graph generation. In *International Conference on Machine Learning (ICML)*, pp. 1630–1639, 2021.

Chen, X., He, J., Han, X., and Liu, L. Efficient and degree-guided graph generation via discrete diffusion modeling. In *International Conference on Machine Learning (ICML)*, pp. 4585–4610, 2023.

Chung, J., Gulcehre, C., Cho, K., and Bengio, Y. Empirical evaluation of gated recurrent neural networks on sequence modeling. In *NIPS Workshop on Deep Learning*, 2014.

Dai, H., Nazi, A., Li, Y., Dai, B., and Schuurmans, D. Scalable deep generative modeling for sparse graphs. In *International Conference on Machine Learning (ICML)*, pp. 2302–2312, 2020.

Dhariwal, P., Jun, H., Payne, C., Kim, J. W., Radford, A., and Sutskever, I. Jukebox: A generative model for music. *arXiv preprint arXiv:2005.00341*, 2020.

- Diestel, R. *Graph Theory*. Electronic library of mathematics. Springer, 2005.
- Dobson, P. D. and Doig, A. J. Distinguishing enzyme structures from non-enzymes without alignments. *Journal of molecular biology*, 330(4):771–783, 2003.
- Fan, A., Lewis, M., and Dauphin, Y. Hierarchical neural story generation. In *Proceedings of the Annual Meeting of the Association for Computational Linguistics (ACL)*, pp. 889–898, 2018.
- Goyal, N., Jain, H. V., and Ranu, S. Graphgen: A scalable approach to domain-agnostic labeled graph generation. In *Proceedings of The Web Conference*, pp. 1253–1263, 2020.
- Gretton, A., Borgwardt, K. M., Rasch, M. J., Schölkopf, B., and Smola, A. A kernel two-sample test. *Journal of Machine Learning Research (JMLR)*, 13(1):723–773, 2012.
- Gu, A. and Dao, T. Mamba: Linear-time sequence modeling with selective state spaces. *arXiv preprint arXiv:2312.00752*, 2023.
- Hagberg, A., Swart, P. J., and Schult, D. A. Exploring network structure, dynamics, and function using networkx. Technical report, Los Alamos National Laboratory (LANL), Los Alamos, NM (United States), 2008.
- Hoogetboom, E., Satorras, V. G., Vignac, C., and Welling, M. Equivariant diffusion for molecule generation in 3d. In *International Conference on Machine Learning (ICML)*, pp. 8867–8887, 2022.
- Huang, R., Li, M., Yang, D., Shi, J., Chang, X., Ye, Z., Wu, Y., Hong, Z., Huang, J., Liu, J., et al. Audiogpt: Understanding and generating speech, music, sound, and talking head. In *Proceedings of the AAAI Conference on Artificial Intelligence*, pp. 23802–23804, 2024.
- Ingraham, J., Garg, V., Barzilay, R., and Jaakkola, T. Generative models for graph-based protein design. In *Advances in Neural Information Processing Systems (NeurIPS)*, volume 32, 2019.
- Ivanov, S. and Burnaev, E. Anonymous walk embeddings. In *International Conference on Machine Learning (ICML)*, 2018.
- Jain, S. M. Hugging face. In *Introduction to transformers for NLP: With the hugging face library and models to solve problems*, pp. 51–67. Springer, 2022.
- Jin, W., Barzilay, R., and Jaakkola, T. Junction tree variational autoencoder for molecular graph generation. In *International Conference on Machine Learning (ICML)*, 2018.
- Jo, J., Lee, S., and Hwang, S. J. Score-based generative modeling of graphs via the system of stochastic differential equations. In *International Conference on Machine Learning (ICML)*, pp. 10362–10383, 2022.
- Karami, M. Higen: Hierarchical graph generative networks. In *International Conference on Learning Representations (ICLR)*, 2024.
- Kim, J., Zaghen, O., Suleymanzade, A., Ryou, Y., and Hong, S. Revisiting random walks for learning on graphs. *arXiv preprint arXiv:2407.01214*, 2024.
- Kipf, T. N. and Welling, M. Variational graph auto-encoders. *arXiv preprint arXiv:1611.07308*, 2016.
- Kong, L., Cui, J., Sun, H., Zhuang, Y., Prakash, B. A., and Zhang, C. Autoregressive diffusion model for graph generation. In *International Conference on Machine Learning (ICML)*, pp. 17391–17408, 2023.
- Kwon, Y., Lee, D., Choi, Y.-S., Shin, K., and Kang, S. Compressed graph representation for scalable molecular graph generation. *Journal of Cheminformatics*, 12:1–8, 2020.
- Li, Y., Vinyals, O., Dyer, C., Pascanu, R., and Battaglia, P. Learning deep generative models of graphs. *arXiv preprint arXiv:1803.03324*, 2018.
- Liao, R., Li, Y., Song, Y., Wang, S., Hamilton, W., Duvenaud, D. K., Urtasun, R., and Zemel, R. Efficient graph generation with graph recurrent attention networks. In *Advances in Neural Information Processing Systems (NeurIPS)*, 2019.
- Lim, J., Hwang, S.-Y., Moon, S., Kim, S., and Kim, W. Y. Scaffold-based molecular design with a graph generative model. *Chemical Science*, 11(4):1153–1164, 2020.
- Martinkus, K., Loukas, A., Perraudin, N., and Wattenhofer, R. Spectre: Spectral conditioning helps to overcome the expressivity limits of one-shot graph generators. In *International Conference on Machine Learning (ICML)*, pp. 15159–15179, 2022.
- Maziarz, K., Jackson-Flux, H. R., Cameron, P., Sirockin, F., Schneider, N., Stiefl, N., Segler, M., and Brockschmidt, M. Learning to extend molecular scaffolds with structural motifs. In *International Conference on Learning Representations (ICLR)*, 2022.
- Mercado, R., Rastemo, T., Lindelöf, E., Klambauer, G., Engkvist, O., Chen, H., and Bjerrum, E. J. Graph networks for molecular design. *Machine Learning: Science and Technology*, 2(2):025023, 2021.

- Neumann, M., Moreno, P., Antanas, L., Garnett, R., and Kersting, K. Graph kernels for object category prediction in task-dependent robot grasping. In *Online proceedings of the eleventh workshop on mining and learning with graphs*, pp. 0–6. ACM Chicago, Illinois, USA, 2013.
- Nikolentzos, G. and Vazirgiannis, M. Random walk graph neural networks. In *Advances in Neural Information Processing Systems (NeurIPS)*, volume 33, pp. 16211–16222, 2020.
- Niu, C., Song, Y., Song, J., Zhao, S., Grover, A., and Ermon, S. Permutation invariant graph generation via score-based generative modeling. In *International Conference on Artificial Intelligence and Statistics (AISTATS)*, pp. 4474–4484, 2020.
- O’Bray, L., Horn, M., Rieck, B., and Borgwardt, K. M. Evaluation metrics for graph generative models: Problems, pitfalls, and practical solutions. In *International Conference on Learning Representations (ICLR)*, 2022.
- Polykovskiy, D., Zhebrak, A., Sanchez-Lengeling, B., Golovanov, S., Tatanov, O., Belyaev, S., Kurbanov, R., Artamonov, A., Aladinskiy, V., Veselov, M., et al. Molecular sets (moses): a benchmarking platform for molecular generation models. *Frontiers in pharmacology*, 11:565644, 2020.
- Radford, A., Wu, J., Child, R., Luan, D., Amodei, D., Sutskever, I., et al. Language models are unsupervised multitask learners. *OpenAI blog*, 1(8):9, 2019.
- Rombach, R., Blattmann, A., Lorenz, D., Esser, P., and Ommer, B. High-resolution image synthesis with latent diffusion models. In *Proceedings of the Conference on Computer Vision and Pattern Recognition (CVPR)*, pp. 10684–10695, 2022.
- Shazeer, N. Glu variants improve transformer. *arXiv preprint arXiv:2002.05202*, 2020.
- Simonovsky, M. and Komodakis, N. Graphvae: Towards generation of small graphs using variational autoencoders. In *International Conference on Artificial Neural Networks*, pp. 412–422, 2018.
- Su, J., Ahmed, M., Lu, Y., Pan, S., Bo, W., and Liu, Y. Roformer: Enhanced transformer with rotary position embedding. *Neurocomputing*, 568:127063, 2024.
- Thompson, R., Knyazev, B., Ghaleb, E., Kim, J., and Taylor, G. W. On evaluation metrics for graph generative models. In *International Conference on Learning Representations (ICLR)*, 2022.
- Tian, K., Jiang, Y., Yuan, Z., Peng, B., and Wang, L. Visual autoregressive modeling: Scalable image generation via next-scale prediction. In *Advances in Neural Information Processing Systems (NeurIPS)*, 2024.
- Tönshoff, J., Ritzert, M., Wolf, H., and Grohe, M. Walking out of the weisfeiler leman hierarchy: Graph learning beyond message passing. *Transactions on Machine Learning Research (TMLR)*, 2023.
- Touvron, H., Lavril, T., Izacard, G., Martinet, X., Lachaux, M.-A., Lacroix, T., Rozière, B., Goyal, N., Hambro, E., Azhar, F., et al. Llama: Open and efficient foundation language models. *arXiv preprint arXiv:2302.13971*, 2023a.
- Touvron, H., Martin, L., Stone, K., Albert, P., Almahairi, A., Babaei, Y., Bashlykov, N., Batra, S., Bhargava, P., Bhosale, S., et al. Llama 2: Open foundation and fine-tuned chat models. *arXiv preprint arXiv:2307.09288*, 2023b.
- Vaswani, A., Shazeer, N., Parmar, N., Uszkoreit, J., Jones, L., Gomez, A. N., Kaiser, Ł., and Polosukhin, I. Attention is all you need. In *Advances in Neural Information Processing Systems (NeurIPS)*, 2017.
- Vignac, C., Krawczuk, I., Siraudin, A., Wang, B., Cevher, V., and Frossard, P. Digress: Discrete denoising diffusion for graph generation. In *International Conference on Learning Representations (ICLR)*, 2023.
- Wang, Y., Chang, Y.-Y., Liu, Y., Leskovec, J., and Li, P. Inductive representation learning in temporal networks via causal anonymous walks. *arXiv preprint arXiv:2101.05974*, 2021.
- Wu, Z., Ramsundar, B., Feinberg, E. N., Gomes, J., Geniesse, C., Pappu, A. S., Leswing, K., and Pande, V. Moleculenet: a benchmark for molecular machine learning. *Chemical science*, 9(2):513–530, 2018.
- Yin, H., Zhang, M., Wang, Y., Wang, J., and Li, P. Algorithm and system co-design for efficient subgraph-based graph representation learning. *Proceedings of the VLDB Endowment*, 15(11):2788–2796, 2022.
- You, J., Ying, R., Ren, X., Hamilton, W., and Leskovec, J. GraphRNN: Generating realistic graphs with deep auto-regressive models. In *International Conference on Machine Learning (ICML)*, 2018.
- Zhang, B. and Sennrich, R. Root mean square layer normalization. In *Advances in Neural Information Processing Systems (NeurIPS)*, volume 32, 2019.
- Zhao, L., Ding, X., and Akoglu, L. Pard: Permutation-invariant autoregressive diffusion for graph generation. In *Advances in Neural Information Processing Systems (NeurIPS)*, 2024.

Zhao, Q., Ren, W., Li, T., Xu, X., and Liu, H. Graphgpt:
Graph learning with generative pre-trained transformers.
arXiv preprint arXiv:2401.00529, 2023.

Appendix

This appendix provides both theoretical and experimental materials. It is organized as follows: Section A provides additional background on sequence models. Section B provides information about model availability and limitations. Section C provides additional details and remarks on our method. Section D provides proofs for the theorems presented in the main manuscript. Section E provides experimental details. Section F provides additional quantitative and qualitative results.

A. Background on Sequence Model Architectures

Our sequence model architectures are fully based on established natural language models. In particular, we consider three prominent models, including GPT-2 (Radford et al., 2019), LLaMA (Touvron et al., 2023a;b), and Mamba (Gu & Dao, 2023) to demonstrate the effectiveness of our approach. Notably, our methodology is not restricted to these specific models; it can be applied to any sequence or language model.

GPT-2. GPT-2 represents one of the earliest large language models based on the transformer architecture (Vaswani et al., 2017). The model employs pre-normalization with LayerNorm, the GeLU activation function, and absolute positional embeddings to encode token positions in sequences. These design choices laid the foundation for many subsequent models.

LLaMA. LLaMA (Touvron et al., 2023a;b) builds upon the transformer framework with several key enhancements. It incorporates pre-normalization through RMSNorm (Zhang & Sennrich, 2019) and employs the SwiGLU activation function (Shazeer, 2020). Additionally, LLaMA replaces absolute positional embeddings with rotary positional embeddings (Su et al., 2024), enabling better generalization to longer sequences.

Mamba. Mamba (Gu & Dao, 2023) is a state-space model (SSM) that maps input sequences to outputs using continuous-time dynamics. It introduces a selection mechanism that dynamically controls how input data flows into hidden states, making the model parameters adaptive to time and data. This innovation enables Mamba to achieve superior performance compared to other SSMs across various tasks.

B. Availability and Limitations

B.1. Code and Model Availability

Our code and all pre-trained models will be released upon publication.

B.2. Limitations

While AUTOGRAPH demonstrates strong scalability on current graph generation benchmarks, we acknowledge that the datasets used in our study remain relatively small-scale compared to those used in pre-training LLMs. To push the boundaries of more powerful graph generative models or eventually foundation models for graphs, we draw the community’s attention to building more comprehensive graph generation benchmarks and well-curated pre-training datasets.

C. Additional Details about AUTOGRAPH

C.1. Background on Graph Theory

We provide additional background on graph theory necessary for the definitions and theories of SETs and SENTs. The background is largely based on Diestel (2005).

We first give the formal definition of *graph isomorphism*:

Definition C.1 (Graph isomorphism). An isomorphism of graphs G and H is a bijection between the vertex sets of G and H : $\pi : V_G \rightarrow V_H$ such that any two vertices u and v of G are adjacent in G if and only if $\pi(u)$ and $\pi(v)$ are adjacent in H , i.e., $(u, v) \in E_G$ if and only if $(\pi(u), \pi(v)) \in E_H$.

Graph isomorphism is an equivalence relation on graphs and as such it partitions the class of all graphs into equivalence classes. A set of graphs isomorphic to each other is called an isomorphism class of graphs. It is worth noting that our SENT isomorphism also partitions the class of all SENTs into equivalence classes in a similar fashion.

We also provide the formal definition of *induced subgraph*:

Definition C.2 (Induced subgraph). An induced subgraph of a graph is another graph, formed from a subset of the vertices of the graph and all of the edges, from the original graph, connecting pairs of vertices in that subset. Formally, let $S \subseteq V_G$ be any subset of vertices of $G := (V_G, E_G)$. Then, the induced subgraph $G[S]$ is the graph whose vertex set is S and whose edge set consists of all of the edges in E_G that have endpoints in S . That is, for any two vertices $u, v \in S$, $(u, v) \in E_{G[S]}$ if and only if $(u, v) \in E_G$.

C.2. Remarks on Tokenized SENTs

In Section 2.4, we showed that an (ordered) SENT can be converted into a sequence of tokens. Here, we extend this idea by interpreting the tokenized sequence as a random walk on a slightly modified graph. We first introduce an alternative tokenization scheme that is equivalent to the one described earlier but offers enhanced interpretability. The proposed tokenization remains largely unchanged except for how tuples are handled. For each $w = (v, A)$ with $A = \{u_1, \dots, u_p\}$, we now define

$$\text{Token}(w) := [v, <, u_1, <, u_2 \dots, <, u_p, >].$$

We now detail how to modify the original graph G : we introduce three virtual nodes, labeled $/$, $<$, and $>$ respectively. These virtual nodes are connected to all other virtual nodes and original nodes in the graph. This modification ensures that for any non-special token in the tokenized sequence, its subsequent token can either be one of its neighbors or one of the virtual nodes ($/$, $<$, or $>$). Consequently, each token has a direct connection to the node corresponding to the current token, and the language model amounts to learning the state transition functions for these random walks. Since these random walks are non-Markovian, this perspective further justifies our choice of using autoregressive models instead of one-step generative models. Furthermore, as random walks are random sequences on graphs, sampling random walks amounts to sampling from those random sequences.

C.3. Remarks on Model Inference

The model inference is straightforward following the same process as LLMs such as LLaMA (Touvron et al., 2023a;b). An alternative way is to enforce the semantic correctness of the generated sequences of tokens by adjusting the logits at a certain token to obey the semantic rule of the tokenization. For instance, the token ‘ $>$ ’ can only occur after a token ‘ $<$ ’ or no special tokens can appear right after $/$. We manually implemented these transition constraints and incorporated them into the inference. We compared this strategy with the constraint-free counterpart. Surprisingly, our experiments demonstrate that the constraint-free variant could always generate semantically correct tokenized SENTs and perform similarly to the one with the transition constraints. Therefore, we did not use any transition constraints during the inference in our experiments.

D. Proofs

In this section, we provide proof for the theorems stated in the manuscript.

Theorem 2.5. For any SETs $s, t \in \mathcal{S}$, their generated graphs are isomorphic, i.e., $G_s \simeq G_t$, if $s \simeq t$. Conversely, if two graphs $G \simeq H$, then for any SET $s \in \mathcal{S}_G$, there exists a SET $t \in \mathcal{S}_H$ s.t. $s \simeq t$.

Proof of Theorem 2.5. By definition of the isomorphism between s and t , there exists a bijection $\pi : V_s \rightarrow V_t$ s.t. $\pi(s) = t$. Now if $u, v \in V_s$ are adjacent in G_s , i.e., $(u, v) \in E_s$, then $(\pi(u), \pi(v))$ is an edge visited by $\pi(s) = t$, thus $(\pi(u), \pi(v)) \in E_t$. Similarly, the reverse is also true. Consequently, $G_s \simeq G_t$.

Now assume that $G \simeq H$ with an isomorphism π and $s \in \mathcal{S}_G$. It is easy to show that $\pi(s)$ is also a SET and its generated graph $G_{\pi(s)} = H$. By taking $t = \pi(s)$, we obtain the result. \square

Lemma 2.8. For any graph G and SET s in G , the generated graph of any prefix of s is a subgraph of G , but not necessarily an induced subgraph.

Proof of Lemma 2.8. Assume that t is a prefix of s . Then $V_t \subseteq V_s = V_G$ and $E_t \subseteq E_s$. However, G_t is not necessarily an induced subgraph of G_s . We consider the following counter-example: $s = ((1, 2, 3, 4, 1, 3))$, $V_s = \{1, 2, 3, 4\}$, and $E_s = \{(1, 2), (2, 3), (3, 4), (1, 4), (1, 3)\}$. Let $t = ((1, 2, 3, 4, 1))$. t is clearly a prefix of s , but its generated graph is not an induced subgraph of G_s as its generated edge set does contain $(1, 3)$. \square

Theorem 2.14. *For any causal SENT $s \in \mathcal{S}^N$, the generated graph of any prefix t of s is an induced subgraph of G_s if and only if s is semi-hamiltonian. In this case, s is called subgraph-induced.*

Proof of Theorem 2.14. Let us first introduce some notations. We denote by R_s the sequence of the start tuples across all neighborhood trails in s , which is also a neighborhood sequence. By definition of semi-hamiltonian, the occurrences after the first time of a node in s should be in R_s . We denote by $n(s)$ the associated node sequence of SENT s , i.e., $n(s) := n(\|s)$.

Let us first assume that s is semi-hamiltonian.

Assume that t is a prefix of s . It is easy to show that G_t is a subgraph of G_s . Now assume that $u, v \in V_t$ s.t. $(u, v) \in E_s$, we want to show that $(u, v) \in E_t$. There are two cases:

1) Assume that $u, v \in n(t)$. Since s is semi-hamiltonian, $n(s) \setminus n(t)$ either does not contain u or v , or even if one of them, say $u \in n(s) \setminus n(t)$, we have $u \in n(R_s)$ and its associated neighborhood set is empty. In both cases, the edge (u, v) does not belong to the generated edge set of the neighborhood subsequence after $\|t$. By the disjointness of the generated edge sets of s , it can only be included in the generated edge set of t , we thus have $(u, v) \in E_t$.

2) Assume that one of them, say $u \notin n(t)$. There exists a neighborhood set A in a tuple of $\|t$ such as $u \in A$. Since t is causal, we have $u \in n(t)$ which contradicts the assumption.

In all the above cases, we have $(u, v) \in E_t$.

Now let us assume that the generated graph of any prefix of s is an induced subgraph of G_s .

Let us prove that s is semi-hamiltonian by contradiction. Assume that there exist two tuples in $\|s$ with the same nodes $s_i = (v, A_i)$ and $s_j = (v, A_j)$ with $i < j$. There are two cases: 1) $s_j \notin R_s$. A tuple (u, A_u) exists one step before s_j in the same neighborhood trail. We consider the prefix t ending at (u, A_u) . We have $v, u \in V_t$ and $(u, v) \in E_s$, but $(u, v) \notin E_t$, by the disjointness of s and since (u, v) is visited at s_j after t . 2) $s_j \notin R_s$ and $A_j \neq \emptyset$. Since s is causal, there exists $s_u := (u, A_u)$ before s_j s.t. $u \in A_j$. We consider the prefix t ending at exactly this tuple. We have $u, v \in V_t$ and $(u, v) \in E_s$, but $(u, v) \notin E_t$, by the disjointness of s and since (u, v) is an edge visited at (v, A_j) after t . \square

Theorem 2.15. *For $s \in \mathcal{S}_G^N$, s is causal and Hamiltonian if and only if every tuple $w := (v, A_v)$ in $\|s$ satisfies $A_v = \mathcal{N}_G(v) \cap V_s(w)$. In this case, every node is visited exactly once. Moreover, s is causal and semi-hamiltonian if and only if every tuple $w := (v, A_v)$ in s satisfies either $A_v = \mathcal{N}_G(v) \cap V_s(w)$ or $A_v = \emptyset$.*

Proof of Theorem 2.15. Let us first assume that for any tuple $w := (v, A_v)$ in $\|s$, $A_v = \mathcal{N}_G(v) \cap V_s(w)$. Since $A_v \subseteq V_s(w)$ which is a subset of the set of visited nodes, s is causal. Now we prove s is Hamiltonian by contradiction. Assume that there exist two tuples in $\|s$, $s_u := (u, A_u)$ and a later visited one $s_v := (v, A_v)$ s.t. $u = v$. Then, $A_v = \mathcal{N}_G(v) \cap V_s(s_v) = \mathcal{N}_G(u) \cap V_s(s_v)$ should contain the node visited before that is a neighbor of u (either through a trail or the neighborhood set of u), denoted by u' . Thus, the edge (u, u') has been visited twice, which contradicts the disjointness of s .

Assuming that $A_v = \mathcal{N}_G(v) \cap V_s(w)$ or $A_v = \emptyset$ for any tuple (v, A_v) in s , we can also prove s is semi-hamiltonian by contradiction. Assume that there exist two tuples in $\|s$, $s_u := (u, A_u)$ and a later visited one $s_v := (v, A_v)$ s.t. $u = v$ and $A_v \neq \emptyset$. Then, $A_v = \mathcal{N}_G(v) \cap V_s(s_v) = \mathcal{N}_G(u) \cap V_s(s_v)$ by assumption. And using the same argument as above, we have the contradiction.

Now assume that s is causal and Hamiltonian. Let us prove the other direction by contradiction. There exists a tuple $w := (v, A_v)$ in s s.t. $A_v \neq \mathcal{N}_G(v) \cap V_s(w)$. As s is causal, $A_v \subseteq V_s(w)$. $A_v \subseteq \mathcal{N}_G(v)$ as $s \in \mathcal{S}_G^N$. Thus, $A_v \subset \mathcal{N}_G(v) \cap V_s(w)$, which means that there exists $u \in \mathcal{N}_G(v) \cap V_s(w)$ and $u \notin A_v$. Hence, $(u, v) \in E_G$ and u is visited before v . However, as $u \notin A_v$, $(u, v) \in E_G$, and s is Hamiltonian, there exists a tuple (u, A_u) in $\|s$ s.t. $v \in A_u$. By causality of s , v is visited before u , which contradicts the fact that s is Hamiltonian.

Assuming that s is causal and semi-hamiltonian. Let us prove the other direction by contradiction. There exists a tuple $w := (v, A_v)$ in s s.t. $A_v \neq \mathcal{N}_G(v) \cap V_s(w)$ and $A_v \neq \emptyset$. Using the same arguments as above, there exists $(u, v) \in E_G$, and u is visited before v . However, as $u \notin A_v$ and $(u, v) \in E_G$, s should visit the edge (u, v) at some point. Since s is

semi-hamiltonian, if s visits again u, v they can only be the first nodes and their associated neighborhood sets are empty. Hence, there is no means for s to visit (u, v) after v , leading to contradiction. \square

E. Experimental Details

E.1. Datasets

We provide details of the datasets used in our experiments. we adopt the standard train/validation/test splits provided in the original sources. The statistics about the datasets are summarized in Table 11.

Small synthetic graphs: Planar and SBM. Both of these datasets are from Martinkus et al. (2022). The Planar dataset consists of 200 planar graphs with 64 nodes each, generated via Delaunay triangulation on points uniformly sampled in the unit square. The SBM dataset contains 200 graphs comprising 2 to 5 communities, with each community having between 20 and 40 nodes. An edge is placed between two nodes with probability 0.3 if they belong to the same community, and 0.05 otherwise. We follow the same splits as Martinkus et al. (2022).

Large graphs: Proteins and Point Clouds. The Proteins dataset includes graph representations (contact maps) of proteins from Dobson & Doig (2003). In these graphs, each node represents an amino acid, and an edge connects two nodes if their corresponding amino acids are within 6 angstroms of each other. We use the same data splits as Liao et al. (2019). The Point Clouds dataset, also from Liao et al. (2019), consists of 41 point clouds of household objects (Neumann et al., 2013). As many of these graphs are disconnected, we retain only the largest connected component of each, following Bergmeister et al. (2024), and again employ the splits used by Liao et al. (2019).

QM9. The QM9 dataset, from Wu et al. (2018), comprises small molecules with up to nine heavy atoms (carbon, oxygen, nitrogen, and fluorine). In this work, we adopt the more challenging setting proposed by Vignac et al. (2023), where hydrogen atoms are modeled explicitly, and we follow the same data splits as in that reference.

MOSES and GuacaMol. The MOSES and GuacaMol datasets are obtained from the respective benchmark tools of Polykovskiy et al. (2020) and Brown et al. (2019). Both consist of drug-like molecules, with those in GuacaMol typically being larger on average. For each dataset, we convert generated molecular graphs to SMILES using the code from Jo et al. (2022), which permits partial charges. We employ the standard data splits provided by the corresponding benchmarks.

NetworkX. We generate the graphs using the generators from the NetworkX library² (Hagberg et al., 2008), categories including “Classic”, “Lattice”, “Small”, “Random Graphs”, “Geometric”, “Trees”, “Community”, “Social Networks”. We ensure that this dataset *does not contain any graphs in the downstream datasets*. The summary of the code for generating these graphs is provided in Table 12. Notably, the largest graph has up to 5999 nodes.

E.2. Evaluation Metrics

We follow Martinkus et al. (2022) and Vignac et al. (2023) in comparing our model’s performance with other graph generative approaches. Specifically, we measure the maximum mean discrepancy (MMD) between the generated and test graphs for degree distribution, clustering coefficient, orbit counts, and spectrum. As a reference, we also compute these metrics on the training set and report the mean ratio across all properties as a global indicator of statistical discrepancy between the generated samples and test samples. Note that for the Point Clouds dataset, which is defined by a k -nearest-neighbor structure, the degree MMD is always zero and is therefore excluded from the mean ratio. While we utilize these metrics to maintain consistency with previous research, we acknowledge their limitations, particularly regarding arbitrary kernel hyperparameter selection, as highlighted by O’Bray et al. (2022); Thompson et al. (2022).

We additionally track uniqueness and novelty: *uniqueness* is the fraction of generated graphs that are not isomorphic to each other, and *novelty* is the fraction of generated graphs that are not isomorphic to any training graph.

Below, we describe additional metrics specific to each dataset.

²<https://networkx.org/documentation/stable/reference/generators.html>

Table 11. Dataset statistics

DATASET	n_{graphs}			$ V _{\text{max}}$	$ V _{\text{avg}}$	$ E _{\text{max}}$	$ E _{\text{avg}}$
	TRAIN	VAL	TEST				
UNATTRIBUTED GRAPHS							
PLANAR	128	32	40	64	64	181	178
SBM	128	32	40	187	104	1129	500
PROTEINS	587	147	184	500	258	1575	646
POINT CLOUDS	26	7	8	5037	1332	10886	2971
ATTRIBUTED GRAPHS							
QM9	97734	20042	13055	29	18	28	19
MOSES	1584663	176225	176074	27	22	31	23
GUACAMOL	1118633	69926	209654	88	28	88	30
PRE-TRAINING UNATTRIBUTED GRAPHS							
NETWORKX	24957	2516	—	5999	459	5999	751

Planar and SBM. Following Martinkus et al. (2022), we report a *validity score* for synthetic datasets. For Planar graphs, it verifies whether the generated graphs remain planar; for SBM graphs, it measures how likely they are to be generated under the original SBM parameters.

QM9. For QM9, we report the *validity*, *uniqueness*, and *novelty* defined for general molecules, as described in the following paragraph. We also report *atom stability* and *molecule stability* as defined by Hooeboom et al. (2022) and Vignac et al. (2023).

MOSES and GuacaMol. Since MOSES (Polykovskiy et al., 2020) and GuacaMol (Brown et al., 2019) are benchmarking platforms, each comes with its own suite of metrics, which we use to evaluate our model. These include:

- **Validity:** Proportion of molecules passing basic valency checks.
- **Uniqueness:** Proportion of generated molecules with distinct SMILES strings (indicating non-isomorphic structures).
- **Novelty:** Proportion of generated molecules not present in the training set.
- **Filter score:** Proportion of molecules passing the same filters used to create the test set.
- **Fréchet ChemNet Distance (FCD):** Similarity measure between generated and training sets based on learned neural embeddings.
- **SNN:** Similarity to the nearest neighbor, computed via Tanimoto distance.
- **Scaffold similarity:** Comparison of Bemis–Murcko scaffold frequencies.
- **KL divergence:** Differences in the distributions of various physicochemical descriptors.

E.3. Computing Details

We implemented our sequence models using the model hub of Hugging Face. Users can easily test their preferred sequence or language models using our code. Experiments were conducted on a shared computing cluster with various CPU and GPU configurations, including 16 NVIDIA H100 (80GB) GPUs. Each experiment was allocated resources on a single GPU, along with 8 CPUs and up to 48GB of system RAM. The run-time of each model was measured on a single NVIDIA H100 GPU.

E.4. Hyperparameters

Unlike prior studies that adjust model sizes across datasets, we maintain a consistent model architecture and size throughout all experiments, specifically using the small GPT configuration (768 hidden dimensions, 12 layers, 12 attention heads).

Table 12. Summary of the code for generating graphs in the NetworkX dataset

GENERATOR	n_{graphs}	PYTHON CODE
CATEGORY: CLASSIC		
BALANCED TREE	10	<code>nx.balanced_tree(2, np.random.randint(4, 10))</code>
BARBELL GRAPH	100	<code>nx.barbell_graph(np.random.randint(3, 31), np.random.randint(41))</code>
BINOMIAL TREE	10	<code>nx.binomial_tree(np.random.randint(2, 9))</code>
COMPLETE GRAPH	10	<code>nx.complete_graph(np.random.randint(3, 31))</code>
CIRCULAR LADDER GRAPH	300	<code>nx.circular_ladder_graph(np.random.randint(10, 501))</code>
CYCLE GRAPH	2000	<code>nx.cycle_graph(np.random.randint(10, 6001))</code>
DOROGOVITSEV GOLTSEV MENDES GRAPH	5	<code>nx.dorogovtsev_goltsev_mendes_graph(np.random.randint(2, 7))</code>
LADDER GRAPH	500	<code>nx.ladder_graph(np.random.randint(10, 1001))</code>
LOLLIPOP GRAPH	200	<code>nx.lollipop_graph(np.random.randint(3, 21), np.random.randint(10, 51))</code>
STAR GRAPH	200	<code>nx.star_graph(np.random.randint(10, 501))</code>
TURAN GRAPH	100	<code>nx.turan_graph(np.random.randint(10, 41), 2)</code>
WHEEL GRAPH	100	<code>nx.wheel_graph(np.random.randint(10, 201))</code>
CATEGORY: LATTICES		
GRID 2D GRAPH	400	<code>nx.grid_2d_graph(np.random.randint(5, 31), np.random.randint(5, 31))</code>
TRIANGULAR LATTICE GRAPH	400	<code>nx.triangular_lattice_graph(np.random.randint(5, 41), np.random.randint(5, 41))</code>
CATEGORY: SMALL		
ALL BUT THE LCF GRAPH	1 (EACH)	<code>nx.{method}()</code>
CATEGORY: RANDOM GRAPHS		
ERDOS RENYI GRAPH	4000	<code>nx.erdos_renyi_graph(np.random.randint(20, 101), 0.2)</code>
RANDOM REGULAR GRAPH	2000	<code>nx.random_regular_graph(np.random.randint(3, 11), np.random.choice([20, 30, ..., 500]))</code>
BARABASI ALBERT GRAPH	4000	<code>nx.barabasi_albert_graph(np.random.randint(20, 501), np.random.randint(2, 6))</code>
RANDOM LOBSTER	4000	<code>nx.random_lobster(80, 0.7, 0.7)</code>
CATEGORY: GEOMETRIC		
RANDOM GEOMETRIC GRAPH	3000	<code>nx.random_geometric_graph(np.random.choice([20, 30, ..., 100]), 0.3)</code>
WAXMAN GRAPH	2000	<code>nx.waxman_graph(np.random.choice([50, 100, 150, ..., 300]))</code>
CATEGORY: TREES		
RANDOM UNLABELED TREE	1000	<code>nx.random_unlabeled_tree(np.random.randint(20, 501))</code>
CATEGORY: COMMUNITY		
CONNECTED CAVEMAN GRAPH	300	<code>nx.connected_caveman_graph(np.random.randint(10, 101), np.random.randint(2, 5))</code>
WINDMILL GRAPH	300	<code>nx.windmill_graph(np.random.randint(10, 101), np.random.randint(2, 5))</code>
CATEGORY: SOCIAL NETWORKS		
ALL SOCIAL NETWORKS	1 (EACH)	<code>nx.{method}()</code>

Training hyperparameters are aligned with established practices from popular LLMs such as GPT-3 (Brown et al., 2020) and LLaMA (Touvron et al., 2023a). We fix the context length to 2048 and use a batch size of 128 if possible, otherwise 64 for larger graphs. In particular, we employ the AdamW optimizer with a gradient clipping threshold of 1.0, a weight decay of 0.1, and a learning rate schedule with a linear warmup followed by cosine decay, peaking at $6e-4$. The AdamW hyperparameters are set to $\beta = (0.9, 0.95)$. Due to the small dataset sizes of previous benchmarks, we tune the only training hyperparameter dropout in $\{0, 0.5\}$, and find the model achieves better validation loss with the value of 0.5 on the small synthetic datasets.

Inference hyperparameters, including k (top-k sampling) and τ (temperature), are reported in Table 13 and analyzed in detail in Section 4.4 in the main manuscript.

F. Additional Results

F.1. Additional Results on MOSES

Due to space constraints, we provide additional metrics on the MOSES dataset in Table 14.

F.2. Transfer Performance of AUTOGRAPH

We provide here additional results for the transfer learning of AUTOGRAPH. We compare the training curves of AUTOGRAPH models with and without pre-training on the Planar datasets in Figure 4. The result suggests that the model with pre-training converges clearly faster.

F.3. Substructure Conditioned Generation

As presented in Section 4.3, we test more extreme cases by replicating the same motif multiple times before initiating the conditional generation. Figure 5, 6, and 7 demonstrate non-curated samples generated by AUTOGRAPH (trained on the GuacaMol dataset without any additional fine-tuning) conditioned on p copies of the same motif, where $p = 1, 2, 5$

Table 13. Inference hyperparameters for each dataset.

DATASET	W/O PRE-TRAINING		W/ PRE-TRAINING	
	TOP- k	TEMPERATURE τ	TOP- k	TEMPERATURE τ
PLANAR	10	1.0	30	0.9
SBM	60	1.0	150	1.0
PROTEINS	40	1.0	30	1.05
POINT CLOUDS	60	1.0	20	0.9
NETWORKX	120	1.0	—	—
QM9	5	1.0	—	—
MOSES	5	1.0	—	—
GUACAMOL	5	1.0	—	—

Table 14. Comparison of AUTOGRAPH to SOTA methods on the MOSES dataset

MODEL	TYPE	MOSES						
		$n_{\text{graphs}} = 1.58\text{M}, V _{\text{max}} = 27, V _{\text{avg}} \approx 22$						
		VALID \uparrow	UNIQUE \uparrow	NOVEL \uparrow	FILTERS \uparrow	FCD \downarrow	SNN \downarrow	SCAF \uparrow
VAE	SMILES	97.7	99.8	69.5	99.7	0.57	0.58	5.9
JT-VAE	FRAGMENTS	100	100	99.9	97.8	1.00	0.53	10
GRAPHINVENT	GRAPH	96.4	99.8	—	95.0	1.22	0.54	12.7
DiGRESS	GRAPH	85.7	100	95.0	97.1	1.19	0.52	14.8
AUTOGRAPH	GRAPH	87.4	100	85.9	98.6	0.91	0.55	10.2

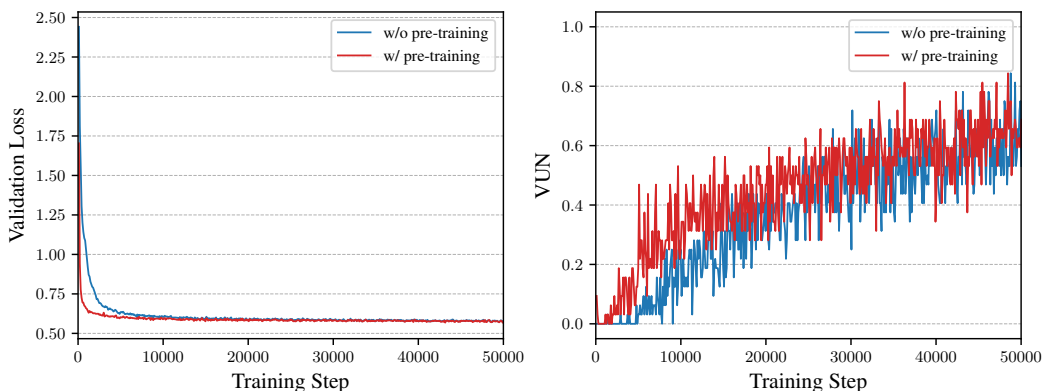


Figure 4. Comparison of AUTOGRAPH with and without pre-training on the Planar dataset with 50000 training steps. The model with pre-training converges clearly faster than the model without pre-training.

respectively.

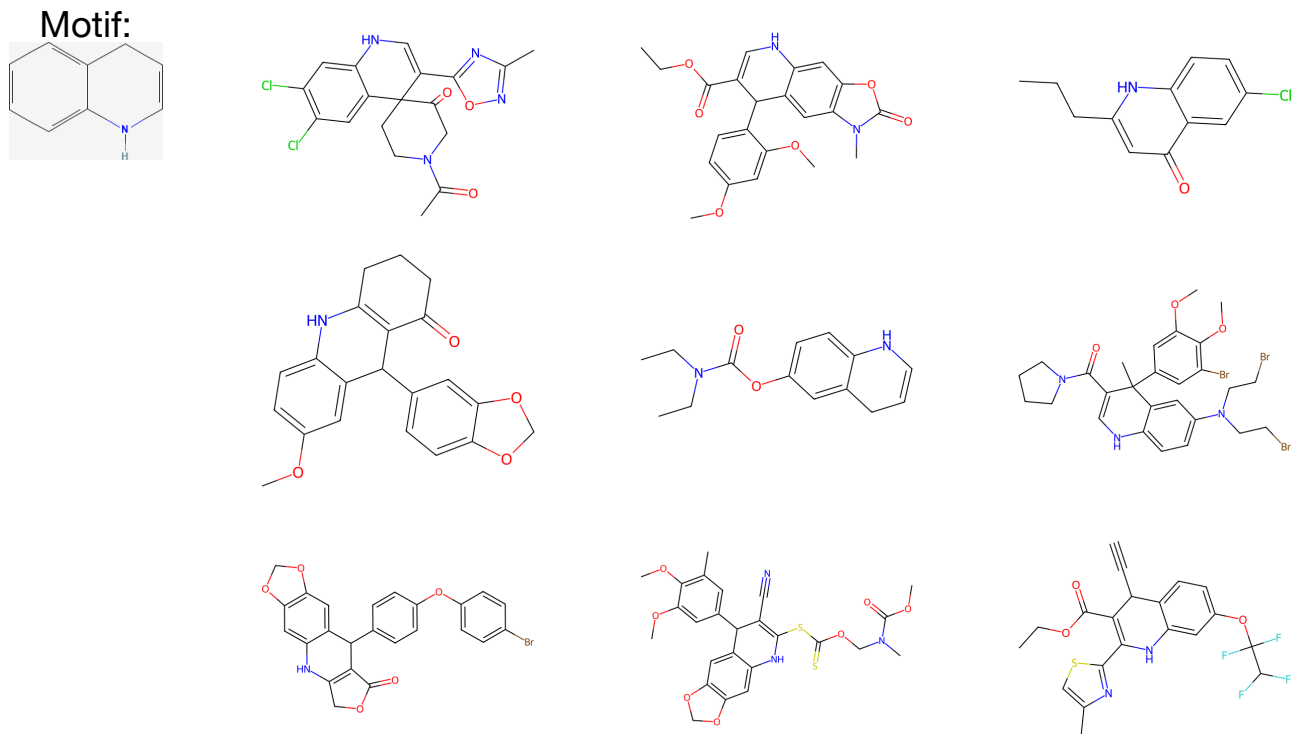


Figure 5. Substructure conditioned generation on one copy of the motif.

F.4. Comparison of Sequence Model Architectures

We provide in Figure 8 the curves of VUN scores vs training steps, which further demonstrates the advantages of transformer-based models compared to state-space models such as Mamba.

F.5. Visualization of Graphs Generated by AUTOGRAPH

F.5.1. RESULTS WITHOUT PRE-TRAINING

We provide visualization of non-curated samples generated by AUTOGRAPH without pre-training on all datasets in Figure 9, 10, 11, 12, 13, 14, and 15. The results on NetworkX are illustrated in Figure 16. Node colors in unattributed graphs represent the eigenvectors associated with the second-smallest eigenvalues of the graph Laplacian.

F.5.2. RESULTS WITH PRE-TRAINING

We provide visualization of non-curated samples generated by AUTOGRAPH with pre-training (on the NetworkX dataset) trained on the non-attributed datasets including Planar, SBM, Proteins, and Point Clouds, illustrated in Figure 17, 18, 19, 20.

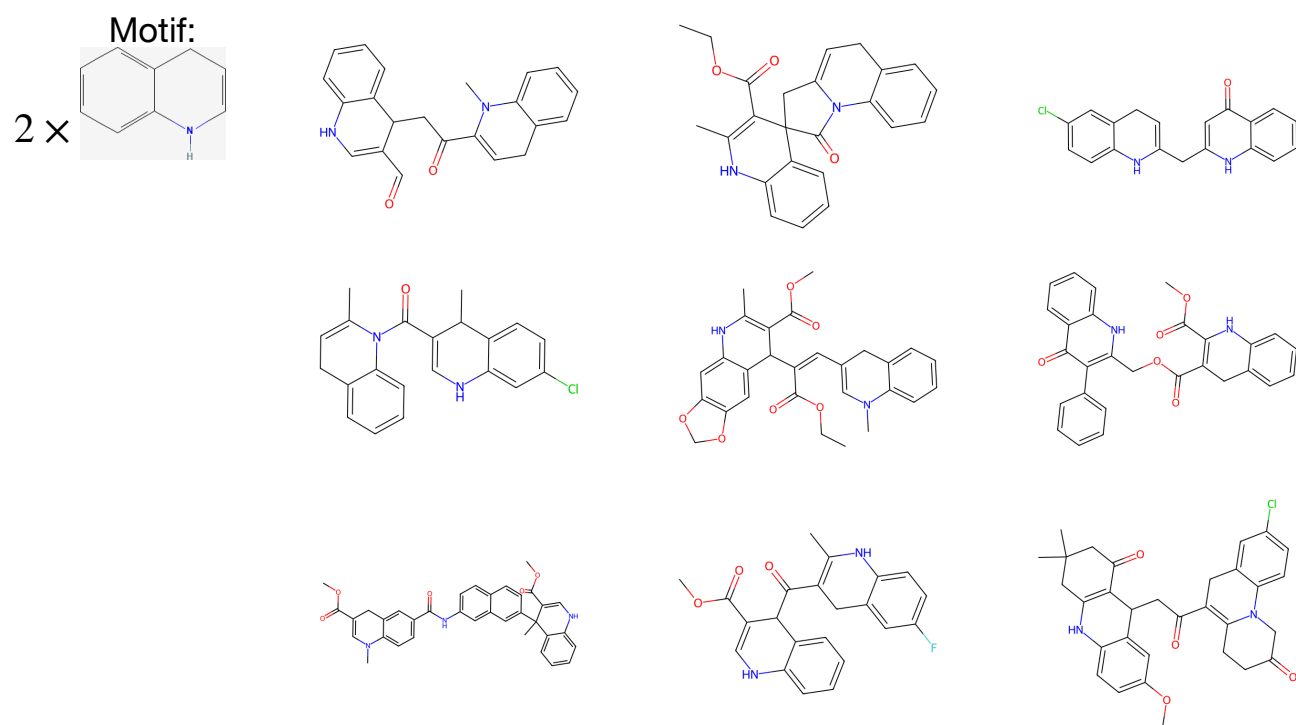


Figure 6. Substructure conditioned generation on two copies of the motif.

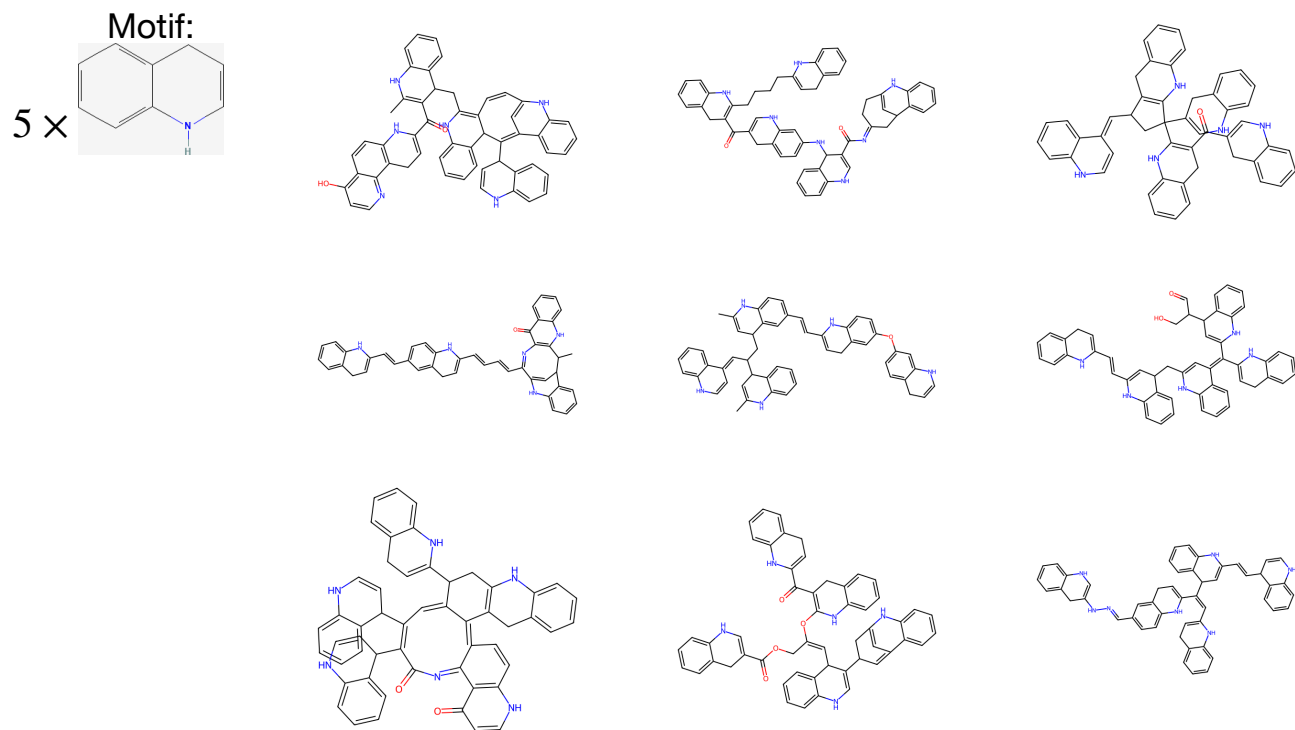


Figure 7. Substructure conditioned generation on five copies of the motif.

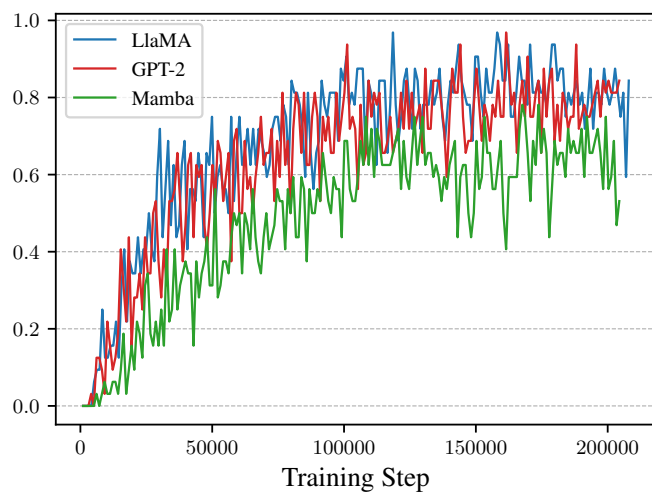


Figure 8. Comparison of sequence model architectures: VUN score vs training steps. Transformer-based models clearly outperform state-space models such as Mamba.

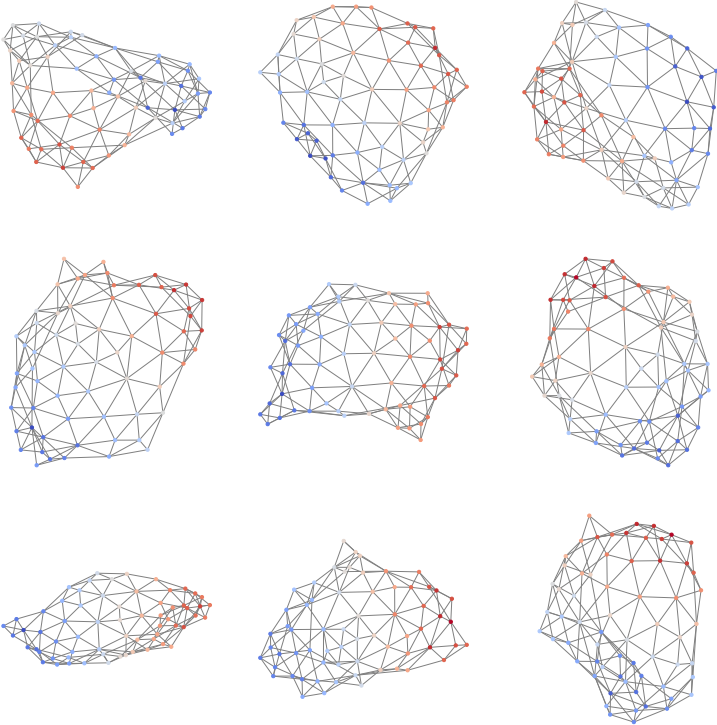


Figure 9. Non-curved samples generated by AUTOGRAPH (without pre-training) trained on the Planar dataset.

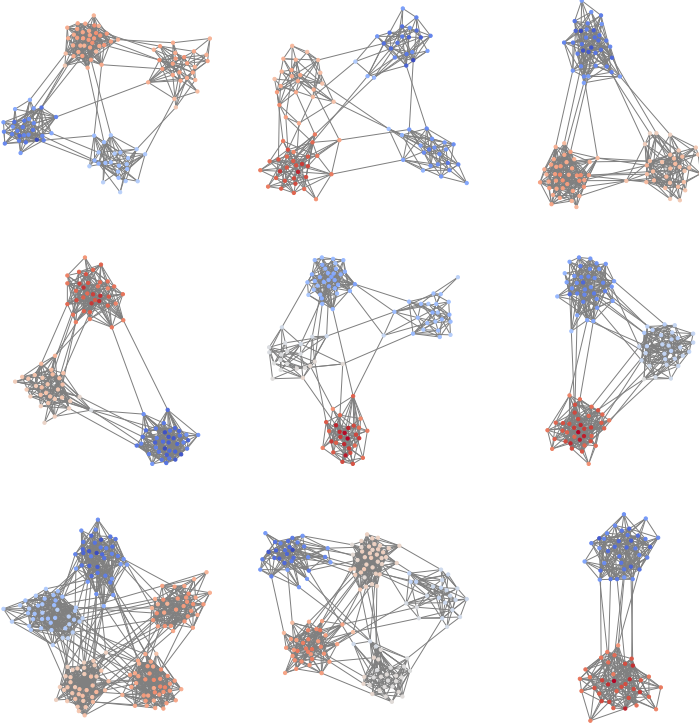


Figure 10. Non-curved samples generated by AUTOGRAPH (without pre-training) trained on the SBM dataset.

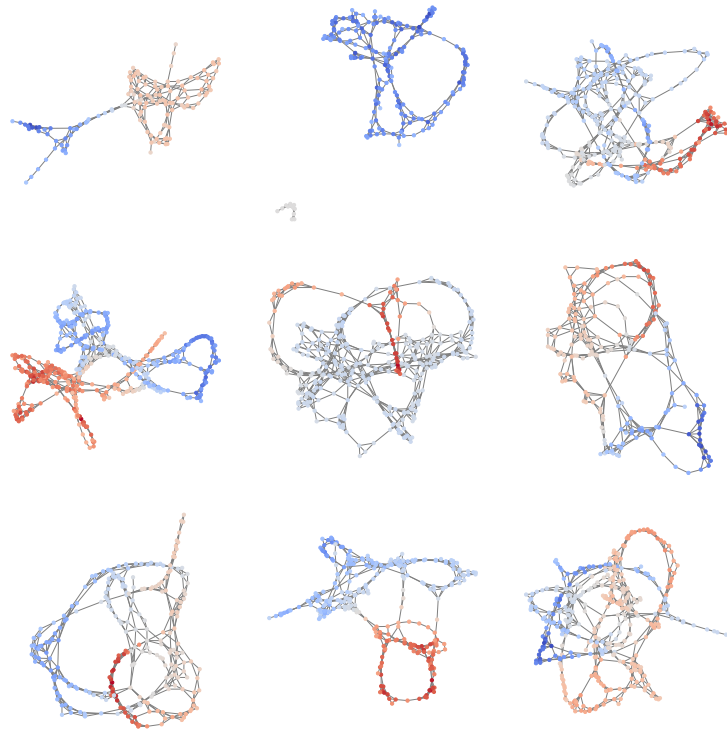


Figure 11. Non-curated samples generated by AUTOGRAPH (without pre-training) trained on the Proteins dataset.

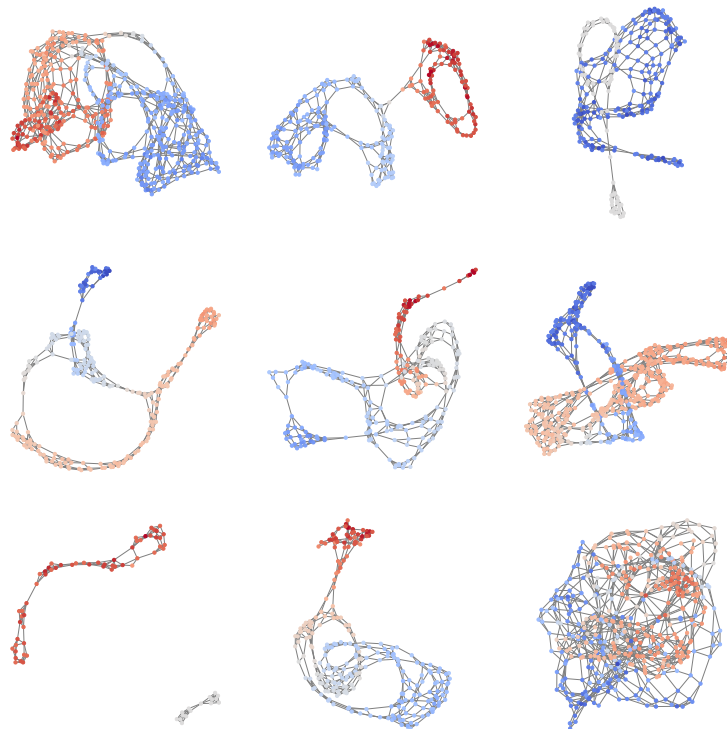


Figure 12. Non-curated samples generated by AUTOGRAPH (without pre-training) trained on the Point Clouds dataset.

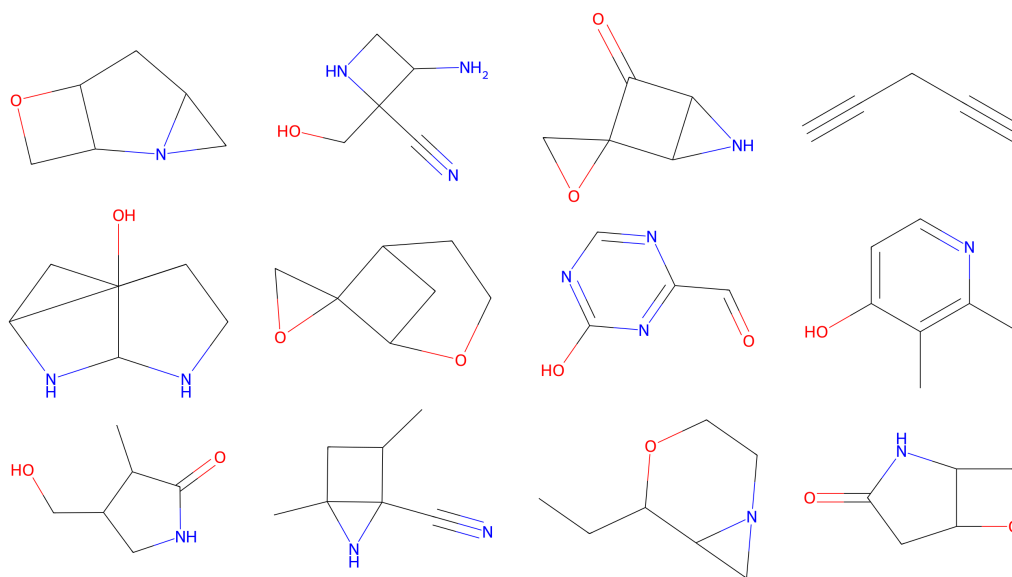


Figure 13. Non-curated samples generated by AUTOGRAPH (without pre-training) trained on the QM9 dataset.

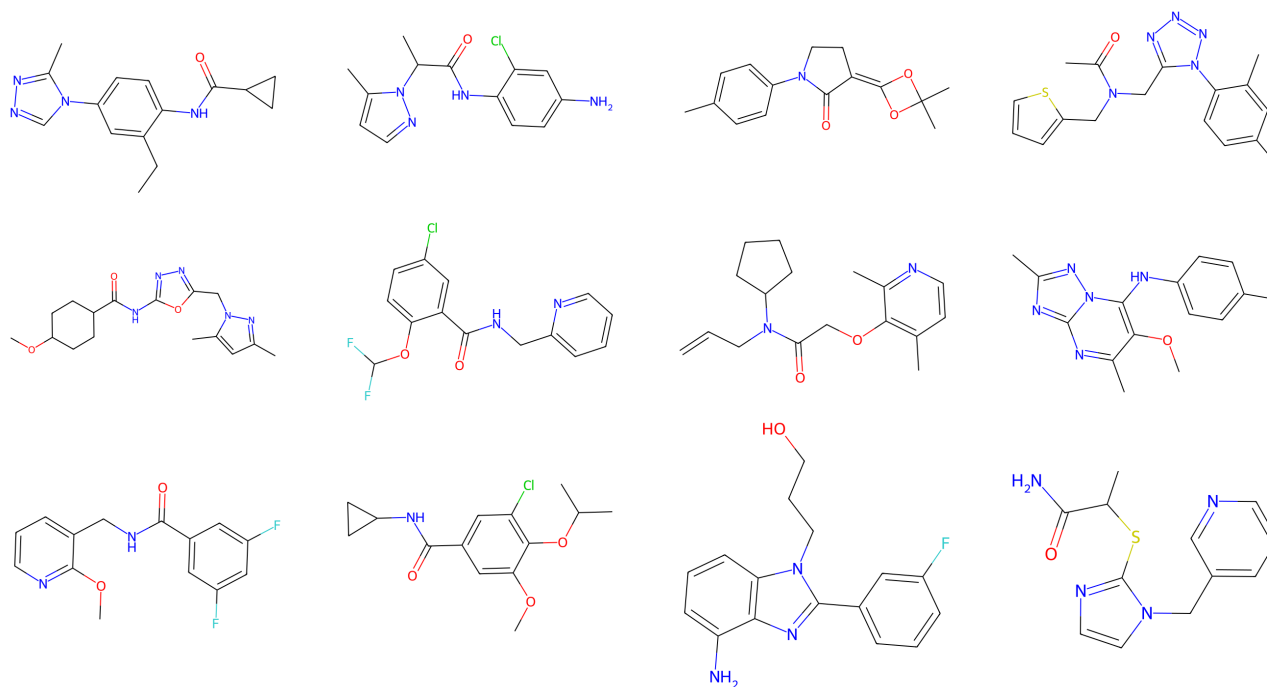


Figure 14. Non-curated samples generated by AUTOGRAPH (without pre-training) trained on the MOSES dataset.

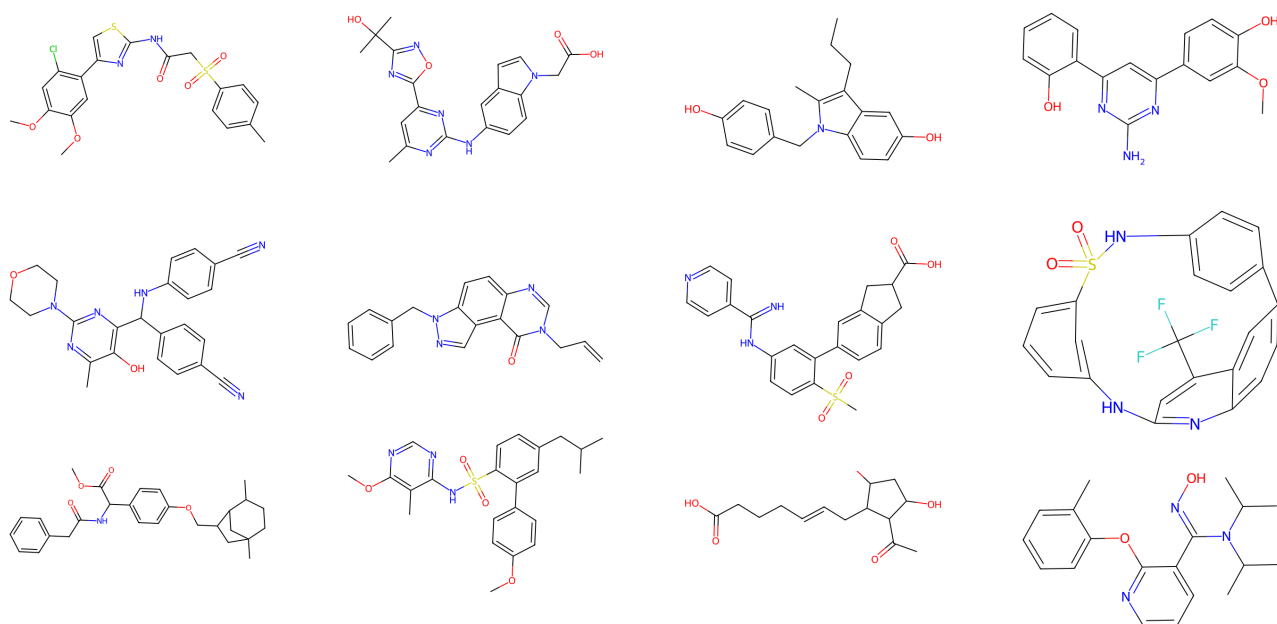


Figure 15. Non-curated samples generated by AUTOGRAPH (without pre-training) trained on the GuacaMol dataset.

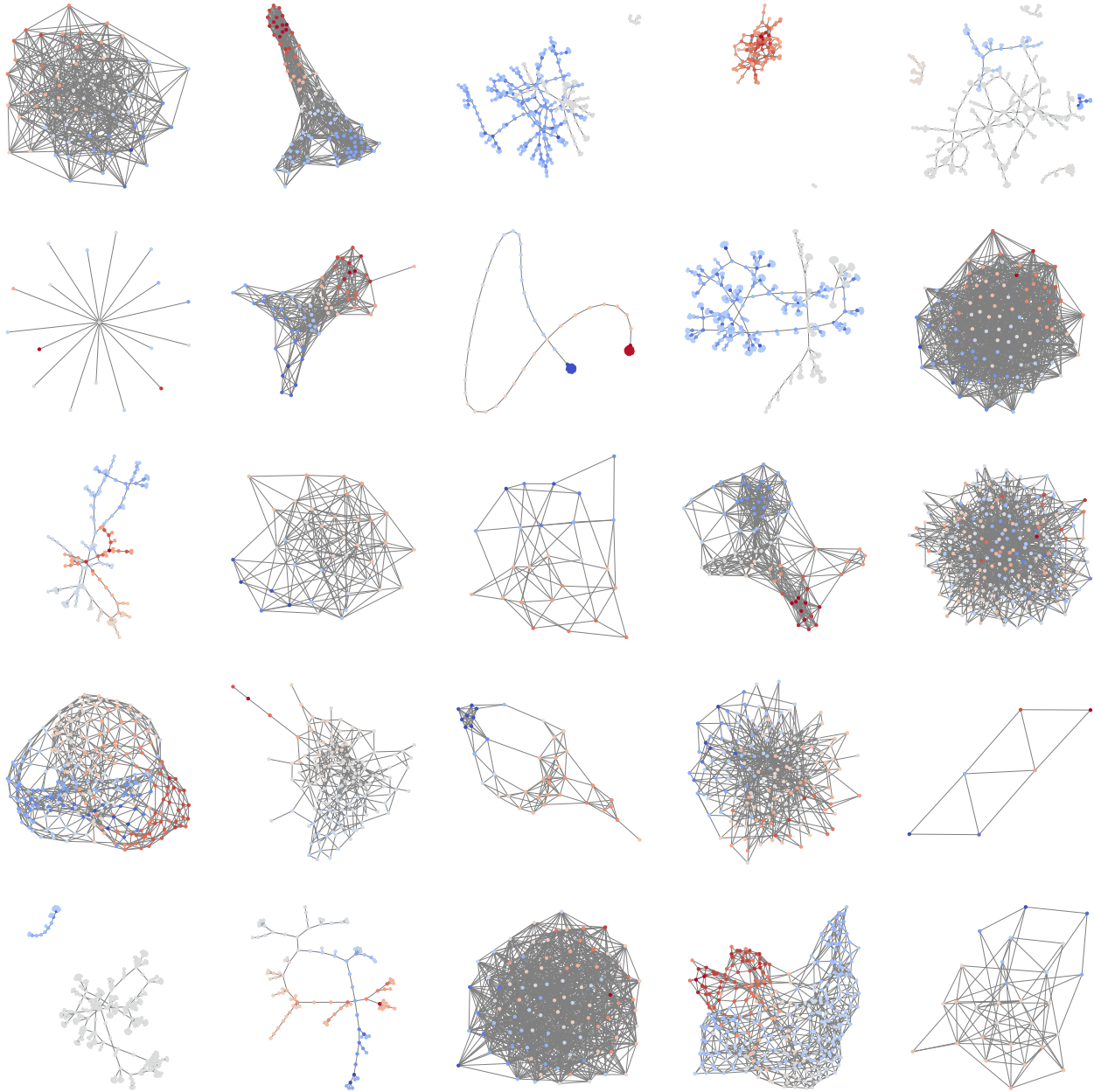


Figure 16. Non-curated samples generated by AUTOGRAPH trained on the NetworkX dataset.

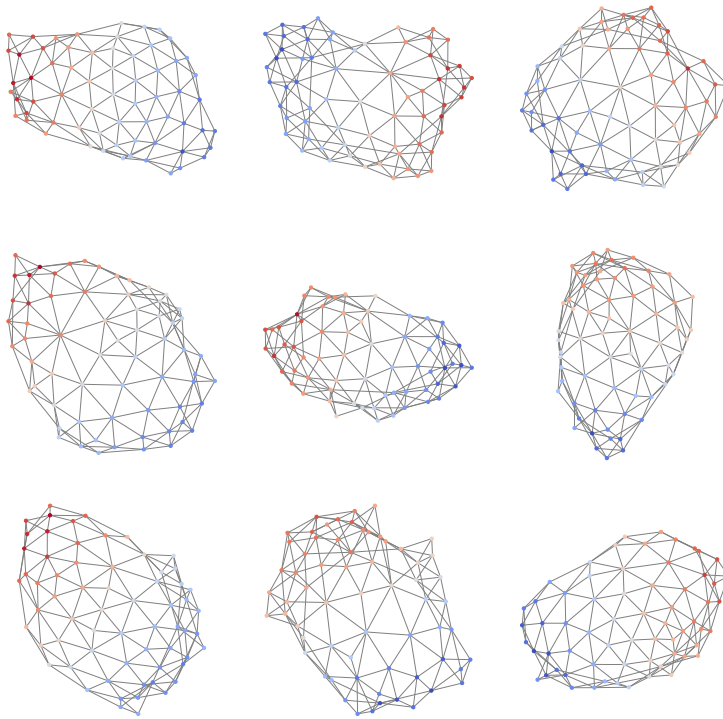


Figure 17. Non-curated samples generated by AUTOGRAPH (with pre-training on the NetworkX dataset) trained on the Planar dataset.

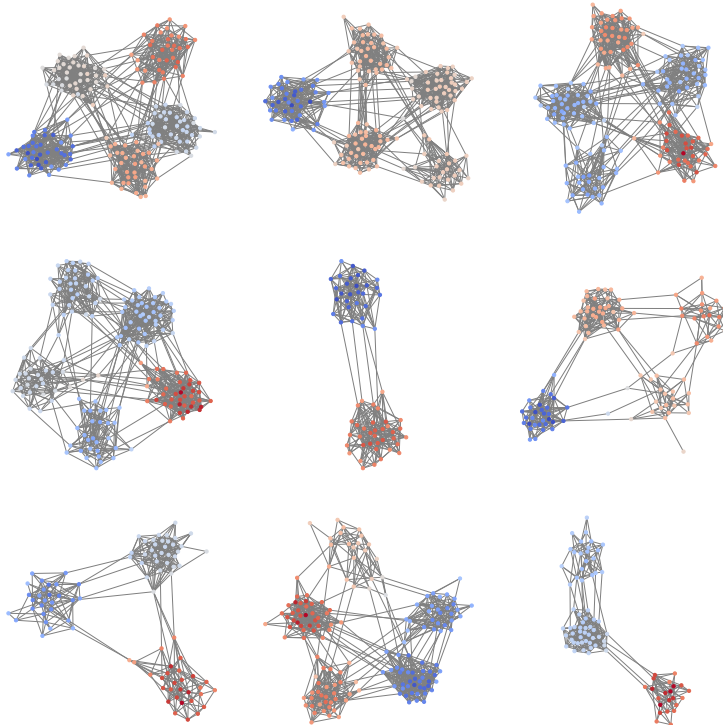


Figure 18. Non-curated samples generated by AUTOGRAPH (with pre-training on the NetworkX dataset) trained on the SBM dataset.

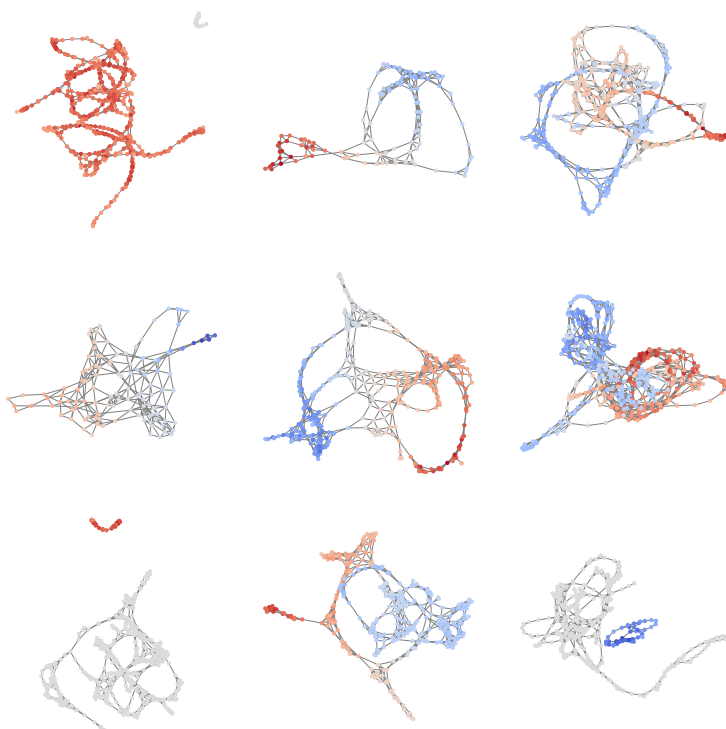


Figure 19. Non-curated samples generated by AUTOGRAPH (with pre-training on the NetworkX dataset) trained on the Proteins dataset.

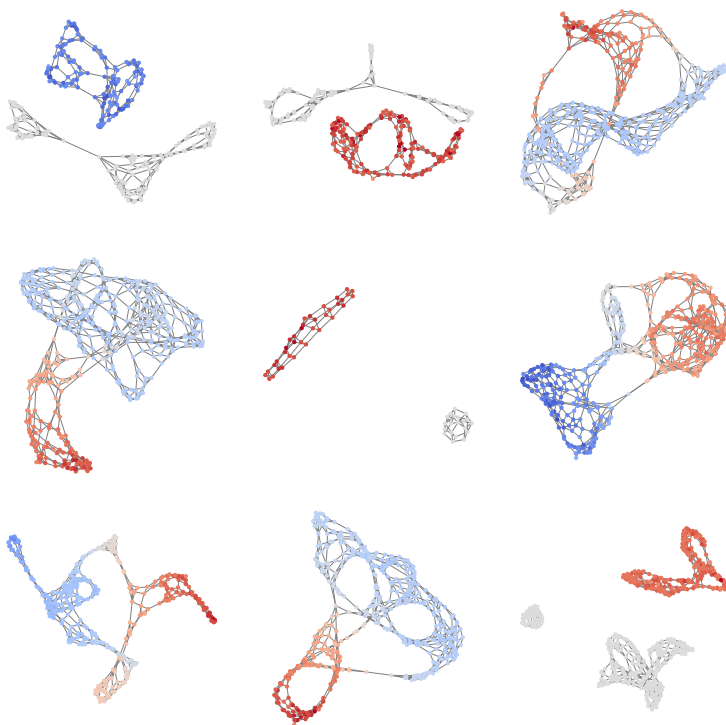


Figure 20. Non-curated samples generated by AUTOGRAPH (with pre-training on the NetworkX dataset) trained on the Point Clouds dataset.